

Article

Experimental and Numerical Investigation of the Behavior of Steel Beams Strengthened by Bolted Hybrid FRP Composites

Omnia R. AbouEl-Hamd ¹, Amr M. I. Sweedan ^{1,*}, Bilal El-Ariss ¹ and Khaled M. El-Sawy ²

¹ Department of Civil and Environmental Engineering, United Arab Emirates University, Al-Ain, Abu Dhabi P.O. Box 15551, United Arab Emirates

² AECOM, Clifton Office, Clifton, NJ 08854, USA

* Correspondence: amr.sweedan@uaeu.ac.ae

Abstract: The strengthening of steel beams using hybrid fiber-reinforced polymers (HFRPs) has gained enormous attention over the last decades. Few researchers have investigated the effectiveness of the fastening techniques without a bonding agent to overcome the undesirable debonding failure of the bonded FRP–steel system. This paper reports the outcomes of experimental and numerical investigations conducted on steel beams strengthened by HFRP using steel bolts. Twenty-two steel beams were tested in four-point loading to investigate the effect of the HFRP length and the bolt arrangement on the flexural behavior of the strengthened systems. The observed failure modes, load–deflection relations, deflection profiles, and strain measurements were also studied. The tested beams showed a ductile behavior, with 15.1 and 22.2% enhancements in the yield and ultimate flexural capacities, respectively. Simplified empirical equations were developed to predict the ultimate load of the bolted HFRP–steel beams. ANSYS software was used to model the beams’ behavior and investigate the effects of the HFRP thickness, bolt spacing, steel grade, loading scheme, and beam length on the effectiveness of the adopted fastening technique. Increasing the HFRP length enhanced the utilization of HFRPs as well as the beam’s ductility, with a reduction of up to 51.2% in the mid-span deflection. Moreover, the strain compatibility of the HFRP–steel beams was improved with an 87.2% reduction in the interfacial slippage. The bolt arrangement showed an insignificant effect on the overall performance of the beams. The numerical results verified the effectiveness of the fastening technique in enhancing the flexural performance of the steel beams, with gains of up to 16.7% and 34.5% in the yield and ultimate load-carrying capacities, respectively.

Keywords: hybrid fiber-reinforced polymers (HFRPs); bolted; strengthening; steel beam; HFRP length; bolt arrangement; finite element; HFRP thickness; steel grade; loading scheme



Citation: AbouEl-Hamd, O.R.; Sweedan, A.M.I.; El-Ariss, B.; El-Sawy, K.M. Experimental and Numerical Investigation of the Behavior of Steel Beams Strengthened by Bolted Hybrid FRP Composites. *Buildings* **2023**, *13*, 824. <https://doi.org/10.3390/buildings13030824>

Academic Editor: Muxuan Tao

Received: 27 February 2023

Revised: 16 March 2023

Accepted: 19 March 2023

Published: 21 March 2023



Copyright: © 2023 by the authors. Licensee MDPI, Basel, Switzerland. This article is an open access article distributed under the terms and conditions of the Creative Commons Attribution (CC BY) license (<https://creativecommons.org/licenses/by/4.0/>).

1. Introduction

The favorable properties of fiber-reinforced polymers (FRPs), including their high strength-to-weight ratio, corrosion resistivity, and light weight make them an attractive material for strengthening steel structures. Extensive research has proven the effectiveness of bonding the FRP composites to structural steel elements for strengthening purposes [1–6]. The debonding failure at the FRP–steel interface poses a continuous challenge in the bonded FRP–steel system as it risks the system’s ductility before utilizing the strength of the bonded FRP. Researchers continuously investigate solutions to overcome the brittle interfacial debonding by exploring the chemical properties of the adhesives and by studying the effects of the bond length, adhesive thickness, and curing time on the performance of the bonded FRP–steel system [7–9]. Various confinement methods were adopted to delay debonding of the FRP from the steel beams [10–13]. Moreover, numerous research studies have investigated the behavior of steel beams strengthened by hybrid bonded–anchored techniques, where end anchors were introduced at the ends of the bonded FRP composites to prevent end debonding. The hybrid bonded–anchored technique delayed the failure

of the system; yet, the system was characterized by the debonding and splitting of the anchored FRP composites [11,14–17]. Recently, shape memory alloys (SMA) were combined with the bonded FRP composites to enhance the performance of the bonded FRP–steel system [18,19].

The brittle nature of the debonding failure, along with the indispensable skillful surface preparation and lengthy curing process of the bonded FRP–steel system, engendered the wish to strengthen the steel elements using unbonded techniques. Several studies were directed towards the exploration of the flexural performance of steel beams strengthened by prestressed FRP laminates attached to the bottom steel flange using end anchorage without bonding agents [10,14,17,20–22]. The studies showed enhanced performance of the strengthened beams; yet, extensive work is required to set the correct profiles of the prestressed CFRP laminates, and a compatible FRP prestressing device is needed to ensure proper stressing of the FRP. The limitations of the bonded and the pre-stressed FRP–steel systems can be avoided simply by fastening the un-prestressed FRP composites along the span of the targeted steel beam. Initial investigations were conducted on bolted FRP–steel joints to explore the behavior of the bolted joints under various fastening conditions [23,24]. The joints showed good bearing with a ductile behavior, proving the ability of the bolted system to overcome the brittle nature of its bonded counterpart. The effects of different fastening conditions on bolted FRP–steel joints were reported throughout the last decade, highlighting the ductile behavior of the bolted system [25–30].

Despite the promising results reported at the joint level of the bolted FRP–steel system, few attempts have been conducted on full-scale beams [31–34]. The experimental behavior of steel beams strengthened by purely bolted FRP composites with different lengths was investigated experimentally [31,34]. The strengthened beams showed a ductile behavior characterized by excessive deflection, bearing in the FRP composites, and local buckling in the compression flanges of the beams, with up to 10.49% and 30.6% enhancements in the yield and ultimate loads, respectively. Analytical and numerical studies were also performed on bolted FRP–steel beams [32,33]. Detailed experimental and numerical analyses of the composite action at the interface of the bolted FRP–steel beams were conducted highlighting the remarkable efficiency of the FRP after steel yielding [32,34]. It is essential to emphasize that adopting the pure fastening technique eliminates the risks associated with the lengthy curing process and the surface preparation of the bonded FRP–steel system. In addition, it excludes the concerns related to the adhesive's type, length, and thickness and its reaction in various weathering conditions. Nevertheless, additional studies are required to validate the adequacy and ductility of the purely bolted FRP–steel system and to verify its effectiveness in strengthening steel beams.

The few cited studies on bolted FRP–steel beams proved the effectiveness of the system in enhancing the ultimate load-carrying capacity of the steel beams while maintaining a ductile performance. However, those studies were limited to the use of either uniform or staggered bolts tested in one loading scheme for a specific steel grade. This research investigates the effectiveness of the bolted system under a wider spectrum of fastening parameters. The effect of the hybrid FRP (HFRP) length is experimentally examined using uniform and staggered bolt arrangements. Failure modes, load-deflection curves, strain measurements, deflection profiles, yield, and ultimate flexural capacities are used to analyze the impact of the investigated parameters. The experimental measurements are used to develop empirical equations that facilitate the prediction of the ultimate load and load-deflection behavior of bolted HFRP–steel beams. A detailed finite element model was also developed to simulate the behavior of the tested specimens and provide a reliable tool to predict the performance of the bolted HFRP–steel beams under various fastening conditions, including HFRP thickness, bolt spacing, steel grade, loading scheme, and beam length. The current study expands the database required to promote the effectiveness of the fastening technique and provides simplified equations to enable the prediction of the performance of the bolted HFRP–steel beams considered in the study.

2. Experimental Study

Twenty-two full-scale steel beams were tested in flexure to investigate the behavior of bolted HFRP–steel beams, utilizing different HFRP lengths and bolt arrangements.

2.1. Material Properties

Two-meter-long UB203x102x23 universal beams with a clear span of 1800 mm were tested in a four-point loading scheme, as depicted in Figure 1. The typical beam cross-section had a total height of 203.75 mm, a flange width of 103.14 mm, a flange thickness of 8.48 mm, and a web thickness of 5.78 mm. To enhance the local stability of the beams during testing, 12 mm thick transverse stiffeners were welded at the mid-span, below the loading points (300 mm from the mid-span on both sides), and at the supports. Additionally, two 12 mm thick endplates were attached at the beam ends. The mechanical properties of the steel material were identified by the tensile testing of six steel coupons (two coupons from the web and two coupons from each flange), following the ASTM-A370-21 standards [35]. The tested coupons showed an average ultimate strength of 620 MPa, a yield strength of 465 MPa, and an elastic modulus of 180 GPa.

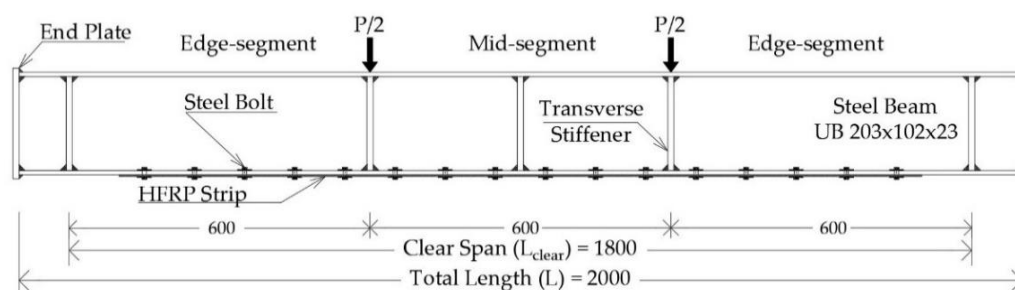


Figure 1. Schematic front view of a typical specimen (dimensions in mm).

Hybrid carbon–glass fiber-reinforced polymers (HFRP) by STRONGWELL[®] were utilized to strengthen the steel beams. The strips had a width of 101.6 mm and a thickness of 3.175 mm. The mechanical properties of the HFRP strips reported by the manufacturer showed an average tensile strength of 852 MPa and a tensile modulus of 62.19 GPa [36]. The HFRP strips were fastened to the bottom flange of the steel specimens using M6 × 40 steel bolts with grade 8.8, as per the DIN ISO 4017 standards [37], 5 mm thick nuts and 2 mm thick washers. The bolts had a shear strength of 375 MPa and a bearing strength of 1000 MPa.

An adjustable ATB 25A breaking-type torque wrench provided by Torqueleader Co., Guildford, UK, was used to tighten the bolted components with 0.1 N.m sensitivity, ±0.04 accuracy, and a torque range from 5 to 25 N.m. The torque wrench was set to 11 N.m, reflecting the value of a calibrated snug-tight condition. Contact-type LVDTs with a capacity of 100 mm were utilized to monitor the vertical and lateral deflections of the beams during testing. The recorded displacements were used to develop the load-deflection curves and the deflection profiles of the different configurations. More details about the experimental programs and the specimens' preparation can be found in [34].

2.2. Methodology and Test Matrix

A description of the test matrix is provided in Table 1, while Figure 2 shows sample schematic views of the main parameters involved. The first component in the specimen designation refers to the bolt arrangement, where “U” indicates a uniform arrangement and “ST” denotes a staggered arrangement. The number next to the letter implies the length of the HFRP strip as a percentage of the beam clear span. Three HFRP lengths were investigated, representing 90, 65, and 45% of the clear span. In the designation, the letter “S” indicates a single HFRP strip, whereas “D” refers to double HFRP strips corresponding to HFRP thicknesses of 3.175 mm and 6.35 mm, respectively. The spacing between the bolts in millimeters (rounded up to the nearest multiple of five) is shown by the number at the end of the designation. In the specimens with uniform bolts, this number refers to the horizontal

spacing. Meanwhile, it presents the slanted distance between the bolts in the staggered arrangement while maintaining a 15 mm spacing between the gauge lines (see Figure 2c). The experimental program involved the investigation of the flexural performance of ten strengthening configurations, with two replicates each, to ensure the repeatability and accuracy of the results. Moreover, two control beams (CBs) were tested to characterize the baseline performance of the un-strengthened beams.

Table 1. Test matrix of the experimental program.

Specimen Designation	Bolt Arrangement	No. of Replicates	HFRP Length (L _{HFRP}) (mm)	HFRP Thickness (mm)	Bolt Spacing (S) (mm)	Number of M6 Bolts
CB	-	2	-	-	-	-
U90S100	Uniform	2	1620	3.175	100	32
U65S100	Uniform	2	1170	3.175	100	24
U45S100	Uniform	2	810	3.175	100	16
U90D35	Uniform	2	1620	6.350	35	96
U65D35	Uniform	2	1170	6.350	35	72
U45D35	Uniform	2	810	6.350	35	48
ST90S100	Staggered	2	1620	3.175	100	32
ST65S100	Staggered	2	1170	3.175	100	24
ST45S100	Staggered	2	810	3.175	100	16
ST90D35	Staggered	2	1620	6.350	35	96

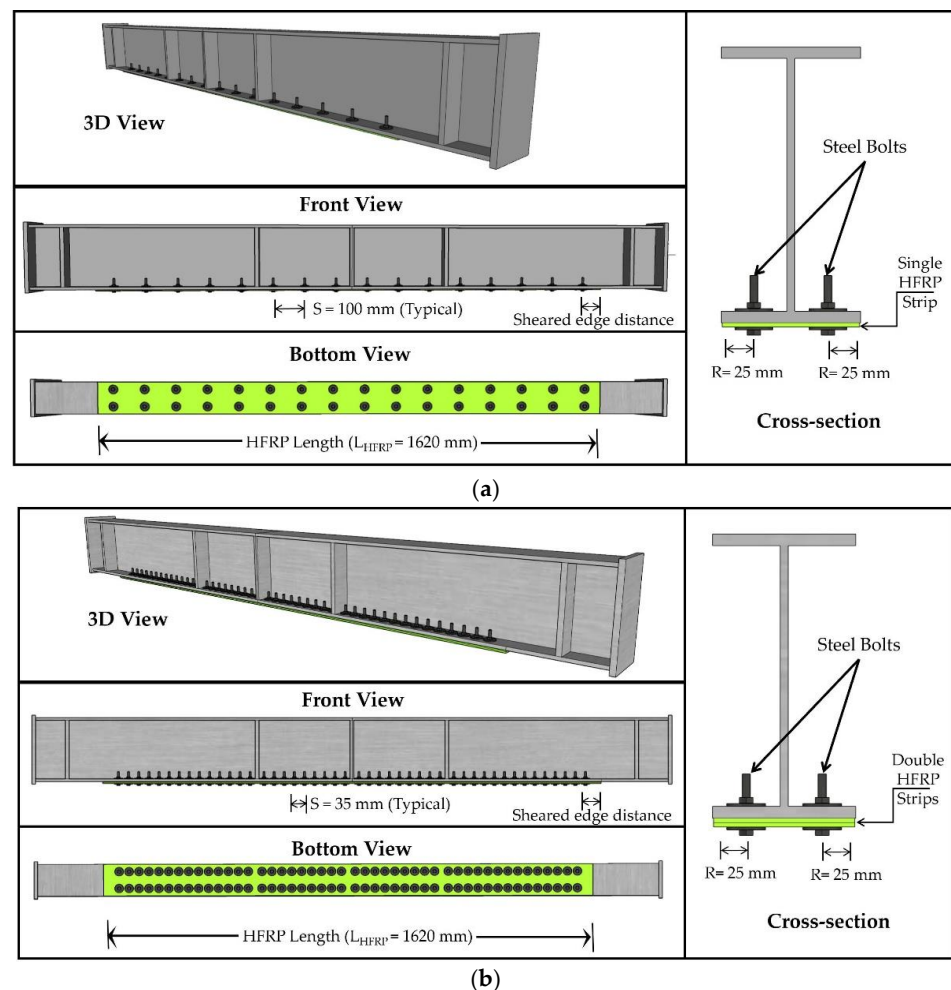
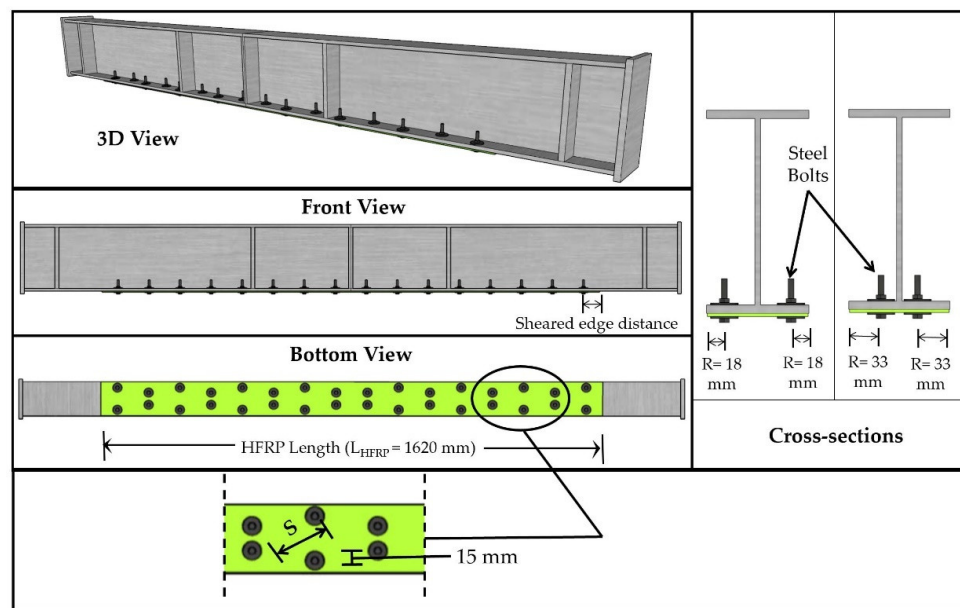


Figure 2. Cont.



(c)

Figure 2. Schematic views of: (a) U90S100; (b) U90D35; (c) ST90S100 specimens.

2.3. Test Set-Up

All HFRP strips had a minimum sheared edge distance “Sh” of 50 mm, as recommended by Sweedan et al. [24]. Meanwhile, rolled edge distances “R” of 25 mm and 18 mm were maintained in all beams with uniform and staggered bolt arrangements, respectively. For illustration purposes, schematic views of selected beams are shown in Figure 2. The steel bolts were used to attach the HFRP strips to the bottom flange while maintaining a proper match between the holes on the HFRP strip and the bottom steel flange, as shown in Figure 3. The beams were simply supported on cylindrical bearing blocks spaced at 1800 mm. A built-up spreader beam was used to transfer the load from the hydraulic actuator to the tested beams while maintaining a spacing of 600 mm between the two loading points (see Figure 4).

All the specimens were instrumented with electrical resistance strain gauges across the beams’ sections and along the HFRP strips. A schematic showing the locations of the strain gauges on U90S100 is displayed in Figure 5. It is worth noting that the numbers and locations of the mounted gauges differed according to the length of the HFRP strip and the spacing between the bolts. After mounting the strain gauges, a protective coat was used to cover the gauges and protect them from exposure to any external effects.



Figure 3. Pictures of fastening the of the HFRP strips to the bottom steel flange.

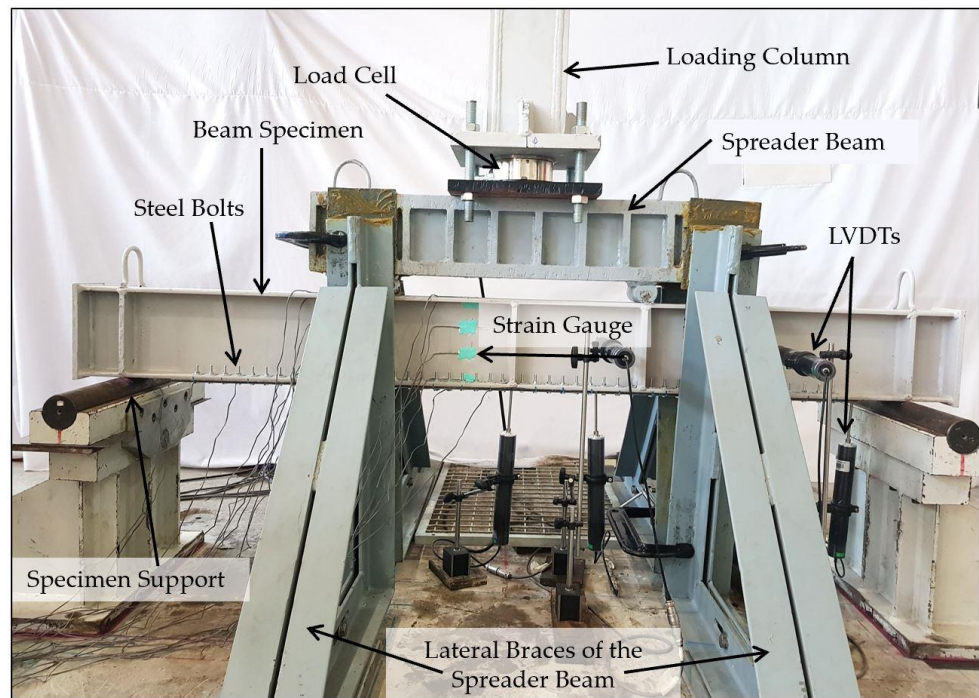


Figure 4. Photo of the test set-up.

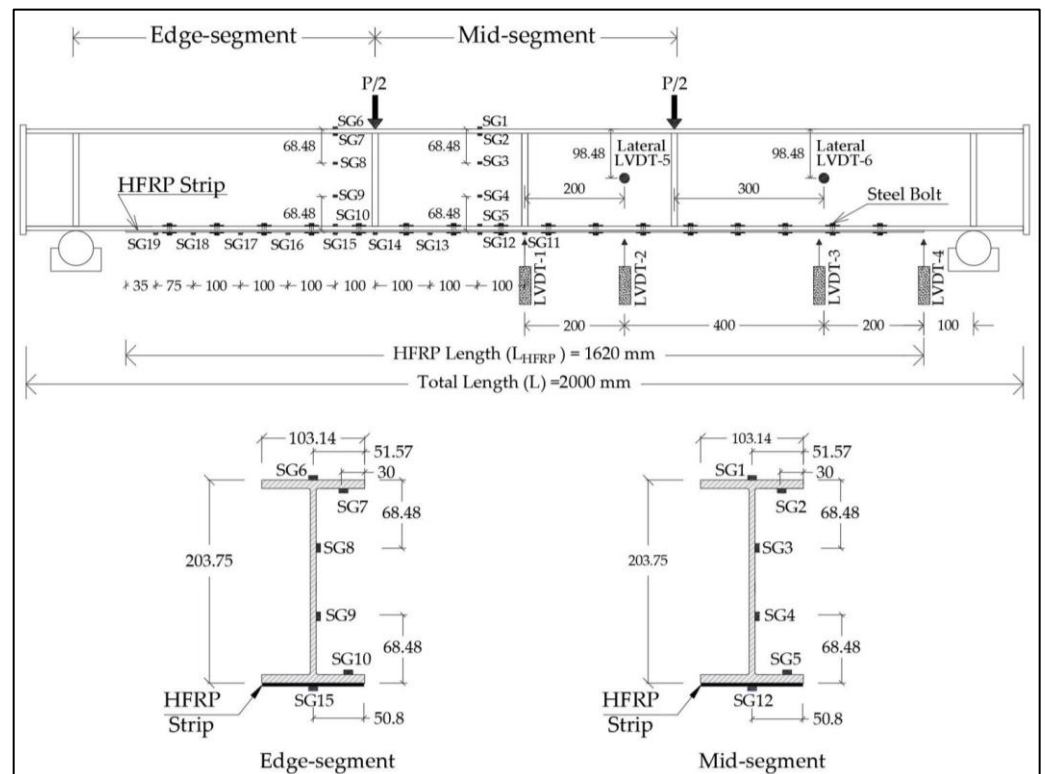


Figure 5. Instrumentation of U90S100 (dimensions in mm).

Six LVDTs were used in each beam to monitor the vertical and lateral displacements during testing (see Figure 5). The vertical deflections at four locations along the beam span were recorded using LVDT-1 to LVDT-4. Additionally, two LVDTs were positioned perpendicular to the beam web to monitor the lateral deflection of the specimens. It is worth mentioning that the load-deflection curve of each specimen was generated using LVDT-1, which was located at the mid-span. A 500 kN MTS hydraulic actuator was used to

apply the load in a displacement-controlled scheme with a rate of 1.5 mm/min. Testing was terminated whenever an excessive deflection of 60 mm was reached or at the failure of the steel bolts.

3. Experimental Results

A discussion of the experimental results is conducted in this section, considering the obtained load-deflection curves, deflection profiles, and strain measurements.

3.1. Failure Modes

The observed failure modes of all the tested specimens, including the un-strengthened control beam (CB), are reported in Table 2. Both replicates of the CB experienced three failure modes, including steel yielding (SY), followed by lateral torsional buckling (LTB), as shown in Figure 6a, and flange local buckling (FLB), as depicted in Figure 6c. The calculated average yield and ultimate flexural strengths of the CB were 78.24 kN.m and 107.4 kN.m, respectively. Fastening the HFRP strips to the bottom flange of the steel beams using steel bolts enhanced the yield and ultimate flexural capacities of the strengthened beams. The calculated enhancement varied according to the strengthening configuration, as displayed in Table 2, with maximum improvement in the yield and ultimate flexural strengths of 15.1% and 22.2%, respectively. All the strengthened beams experienced similar failure modes, including SY, LTB, FLB, and bearing (BR) between the steel bolts and the HFRP strips. In order to visualize the bearing effect, the initial alignment between the bolts and the HFRP strips before testing was marked using a thick marker, as shown in Figure 6b. The slippage resulting from the bearing of the steel bolts on the HFRP during testing was evident by the misalignment of the marks. The ductile behavior of the bolted HFRP strips was noticeable in the sagging of the stretched HFRP strip in U45S100, as displayed in Figure 7, reflecting the ability of the HFRP strips to elongate and to contribute to the ductile behavior of the bolted system.

Table 2. Yield and ultimate flexural strength of tested beams and the associated failure modes.

Specimen Designation	Average M_y (kN.m)	Average M_u (kN.m)	% Increase M_y ^{*a}	% Increase M_u ^{*a}	Failure Modes
CB	78.24	107.40	-	-	SY ^{*b} , LTB ^{*c} , FLB ^{*d}
U90S100	84.94	120.11	8.6	11.8	BR ^{*e} , SY, LTB, FLB
U65S100	82.75	119.79	5.8	11.5	BR, SY, LTB, FLB
U45S100	82.04	117.75	4.9	9.6	BR, SY, LTB, FLB
U90D35	90.03	127.61	15.1	18.8	BR, SY, LTB, FLB
U65D35	86.61	123.56	10.7	15.0	BR, SY, LTB, FLB
U45D35	86.31	116.49	10.3	8.5	BR, SY, BSF ^{*f}
ST90S100	84.89	122.68	8.5	14.2	BR, SY, LTB, FLB
ST65S100	84.14	118.78	7.5	10.6	BR, SY, LTB, FLB
ST45S100	82.32	116.53	5.2	8.5	BR, SY, LTB, FLB
ST90D35	87.83	131.26	12.3	22.2	BR, SY, LTB, FLB

^{*a} %Increase = $100 \times (\text{strengthened beam value} - \text{CB value}) / (\text{CB value})$; ^{*b} SY: steel yielding; ^{*c} LTB: lateral torsional buckling; ^{*d} FLB: flange local buckling; ^{*e} BR: bearing between bolts and HFRP; ^{*f} BSF: bolt shear fracture.

Neither of the replicates of U45D35 experienced major LTB or FLB; yet, they failed by bolt shear fracture (BSF), as shown in Figure 8a, due to the insufficient number of bolts utilized to transfer the interfacial shear from the steel flange to the two short HFRP strips. Once the shear strength of the bolt was reached, the bolt experienced shear fracture, marking the failure of the system. The experimental observations revealed bending in the edge bolts before fracture, as presented in Figure 8b. Despite the undesirable brittle failure of U45D35, average enhancements of 10.3% and 8.5% in the yield and ultimate flexural capacities were calculated compared to the CB.

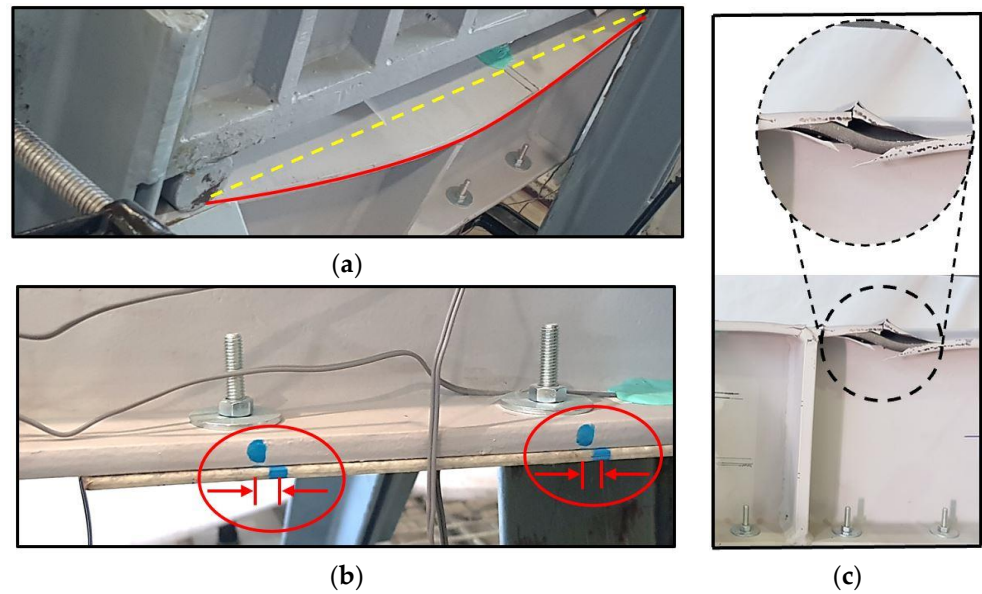


Figure 6. Observed failure modes of the strengthened beams: (a) LTB; (b) bearing of the steel bolts on the HFRP strip; (c) FLB.

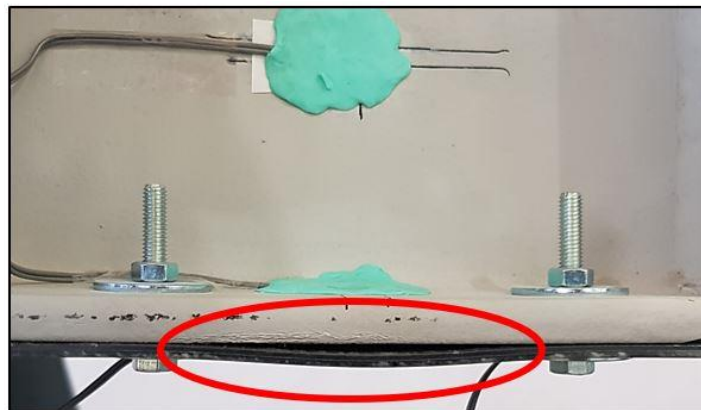


Figure 7. Sagging of the HFRP strip of U45S100.



Figure 8. (a) Shear fracture of the bolts in U45D35; (b) bending of the bolts in U45D35.

3.2. Effect of HFRP Length

The tested specimens were grouped to evaluate the effect of the HFRP length on the beam behavior. The first group includes beams strengthened with a single HFRP strip utilizing steel bolts in a uniform arrangement (i.e., U90S100, U65S100, and U45S100). Meanwhile, the second group focused on the behavior of beams strengthened with double HFRP strips and uniform bolt arrangements (i.e., U90D35, U65D35, and U45D35). Finally, the results of ST90S100, ST65S100, and ST45S100 were used to evaluate the effect of changing

the length of a single HFRP strip fastened using staggered bolts on the performance of the strengthened beams.

3.2.1. Load-Deflection Curves

The load-deflection curves of each of the three groups, along with the CB, are displayed in Figure 9. The plotted curves reveal a ductile behavior of the strengthened beams. The typical load-deflection curve of a tested beam is composed of three main zones: the elastic zone, transitional zone, and plastic zone. The elastic zone shows a linear load-deflection relation with a positive slope reaching the yield load of the respective configuration, where the yielding of the mid-span steel section starts. The reduced slope in the transitional zone of the load-deflection curve is associated with the propagation of yielding across the mid-span section until the full yielding of the section. After that, the beam experienced plastic deformations, where additional loads caused considerably high deflections. The average yield and ultimate flexural strengths of the tested configurations are reported in Table 2.

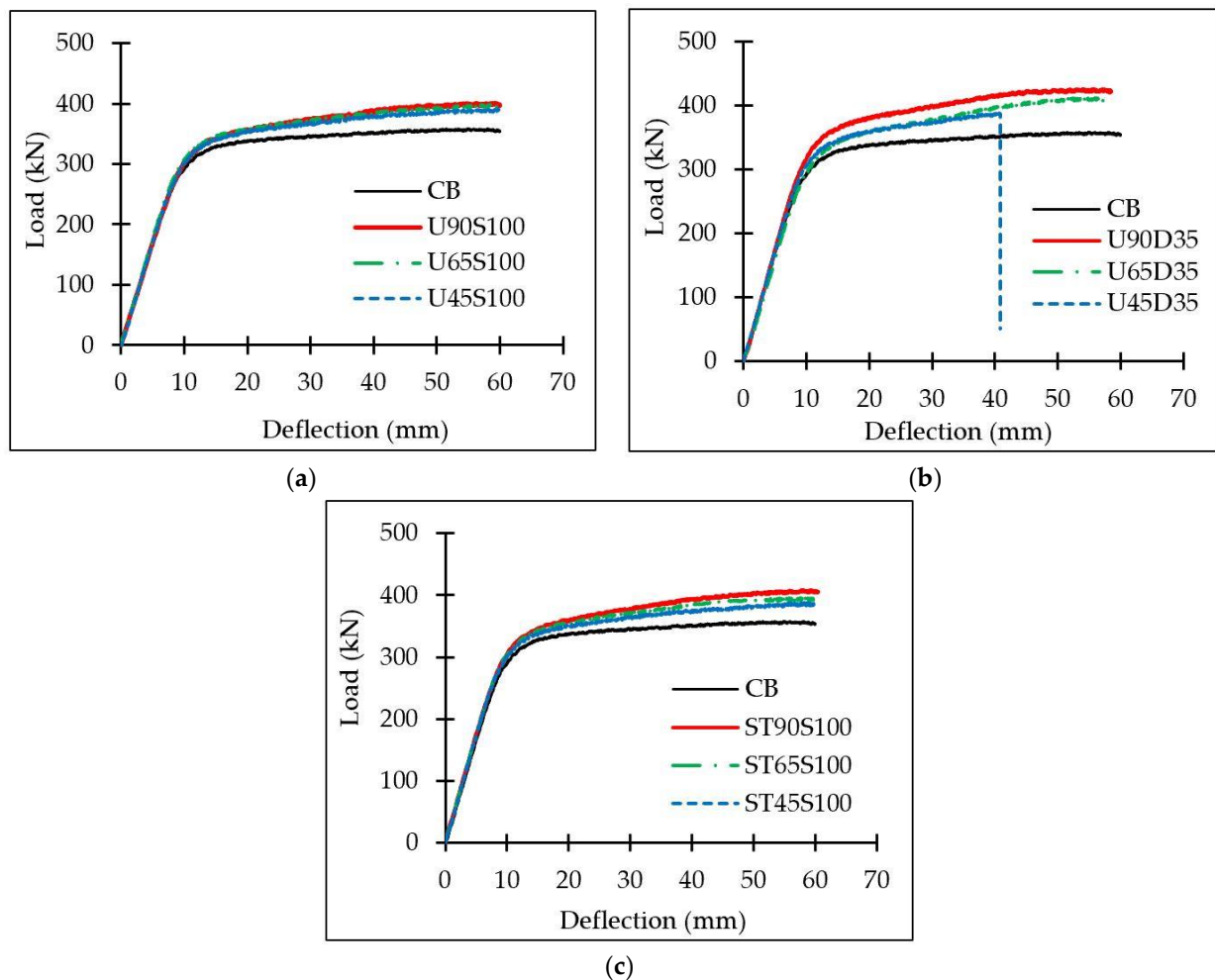


Figure 9. Load-deflection curves of beams with various HFRP lengths adopting: (a) single HFRP strip with uniform steel bolts; (b) double HFRP strips with uniform steel bolts; (c) single HFRP strip with staggered steel bolts.

The beams U45S100, U65S100, and U90S100 showed 4.9%, 5.8%, and 8.6% improvement in the yield capacity compared to the CB, respectively. The load-deflection curves of these specimens in Figure 9a reveal similar ductile behavior, with 11% average enhancement in the ultimate flexural capacity compared to the CB. Although the performance of this group of beams showed considerable improvements in the yield and ultimate flexural

capacities compared to the CB, increasing the length of the HFRP strip from 45% to 90% of the beam span resulted in only 3.5% and 2.0% enhancements in the yield and ultimate strengths, respectively.

The effect of changing the length of the double HFRP strips was also assessed by comparing the average load-deflection curves of U90D35, U65D35, and U45D35 to that of the CB in Figure 9b. The plots reveal a substantial enhancement in the flexural performance of U90D35 and an almost identical performance of U65D35 and U45D35 until a deflection of 30 mm. After that, U65D35 showed a slightly better load-carrying capacity than U45D35 before the BSF (reflected by a sudden drop in the load-deflection curve) took place. The presence of two HFRP strips considerably stiffened the bottom flange, providing a better transfer of loads from the steel flange to the HFRP strips through the steel bolts. However, the number of bolts in specimen U45D35 (with the short HFRP strips) was insufficient to transfer the interfacial shear between the bolted components. It is worth mentioning that the loading of one U45D35 replicate continued after the BSF to observe the post-failure behavior of the bolted system. The experimental observations revealed good re-distribution of the load among the remaining intact bolts, enabling an additional 20 mm deflection before the spreading of the bolts' fractures. Despite the brittle failure of U45D35, all the replicates of U90D35 and U65D35 showed ductile behavior during testing implying better ductility with the increased HFRP length. The calculated average enhancements in the ultimate flexural capacities of U65D35 and U90D35 compared to the CB were 15.0% and 18.8%, respectively. Increasing the length of the double HFRP strips, fastened by uniformly distributed steel bolts from 45% to 90% of the beam span, improved the yield and ultimate flexural capacities of the strengthened beams by 4.3% and 9.5%, respectively.

The load-deflection curves of the beams strengthened by different lengths of a single HFRP strip bolted by staggered steel bolts are displayed in Figure 9c. The plots highlight the improved performance associated with increasing the length of the HFRP strip. The beams ST45S100, ST65S100, and ST90S100 showed 5.2%, 7.5%, and 8.5% enhancements in the yield load compared to the CB, respectively (refer to Table 2). Meanwhile, the calculated improvements in the ultimate loads of ST45S100, ST65S100, and ST90S100 compared to the CB were 8.5%, 10.6%, and 14.2%, respectively. Increasing the length of a single HFRP strip bolted by staggered steel bolts from 45% to 90% of the beam span slightly improved the yield and ultimate loads of the strengthened beams by 3.1% and 5.3%, respectively.

3.2.2. Deflection Profiles

The effect of the HFRP length on the serviceability, in terms of the deflection, was assessed by comparing the deflection profiles along the span of the grouped beams at a fixed load value of 380 kN, which is slightly lower than the peak load of all the beams, as shown in Figure 10. Increasing the length of the HFRP strip reduced the beam deflection, implying better serviceability, which was more notable at high loads. It is worth noting that the mid-span deflection of U90S100 at 380 kN (see Figure 10a) was 28.7% lower than that of U45S100. Similarly, the mid-span deflection of U90D35 showed lower measurements than that of U45D35 by 51.2% (refer to Figure 10b). Moreover, the measured mid-span deflection of ST90S100 at 380 kN was less than that of ST45S100 by 30% (see Figure 10c). Increasing the length of the HFRP strip increased the number of utilized steel bolts at the bottom flange and, consequently, enhanced the system's stiffness and resulted in lower deflection at high loads.

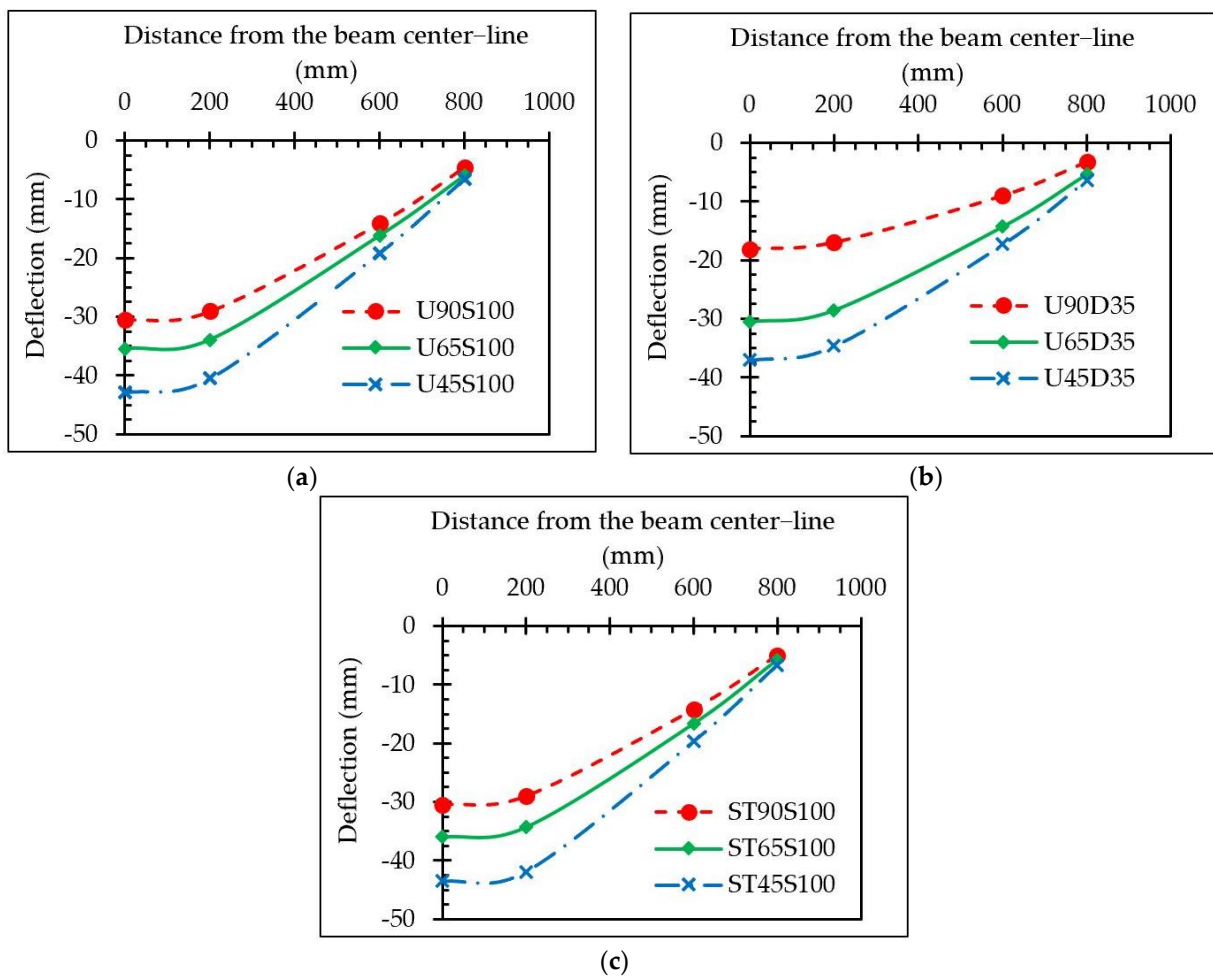


Figure 10. Effect of HFRP length on the deflection profiles of beams strengthened by: (a) single HFRP strip with uniform steel bolts; (b) double HFRP strips with uniform steel bolts; (c) single HFRP strip with staggered steel bolts.

3.2.3. Strain Measurements

The effect of the HFRP length on the tensile strains of the strengthened beams was analyzed in view of the strain profiles along the depth of the beam. The measured tensile strains at the mid-segment and edge-segment of U90S100, U65S100, U45S100, and the CB at 310 kN are plotted in Figure 11. The bolted HFRP strips effectively reduced the strains in the tension side compared to the CB. It is visible in Figure 11 that the effectiveness of the bolted HFRP strips in reducing the tensile strains was more pronounced at the mid-segment than at the edge-segment. This observation implies that the combined shear and flexure stresses at the edge-segment limit the effectiveness of the bolted HFRP in enhancing the flexural performance of the strengthened beams. The % utilization of the HFRP strength ($\%U_{\sigma_{\text{HFRP}}}$), as displayed in Table 3, is calculated as follows:

$$\%U_{\sigma_{\text{HFRP}}} = \frac{\sigma_{\text{HFRP},x}}{\sigma_{\text{HFRP,max}}} \times 100 = \frac{E_{\text{HFRP}} \varepsilon_{\text{HFRP},x}}{\sigma_{\text{HFRP,max}}} \times 100 \quad (1)$$

where $\sigma_{\text{HFRP},x}$ is the HFRP stress at a specified load; $\sigma_{\text{HFRP,max}}$ is the tensile stress of the HFRP (852 MPa); E_{HFRP} is the tensile modulus of the HFRP (62.19 GPa); and $\varepsilon_{\text{HFRP},x}$ is the measured strain at the HFRP strips at a specific load. The tabulated $\%U_{\sigma_{\text{HFRP}}}$ values show a higher contribution of the HFRP at the mid-segment than the edge-segment for all the configurations. Table 3 also indicates a better utilization of the bolted HFRP strip in the

beams with a longer HFRP, as doubling the HFRP length almost doubled the $\%U_{\sigma\text{HFRP}}$ at the mid-segment.

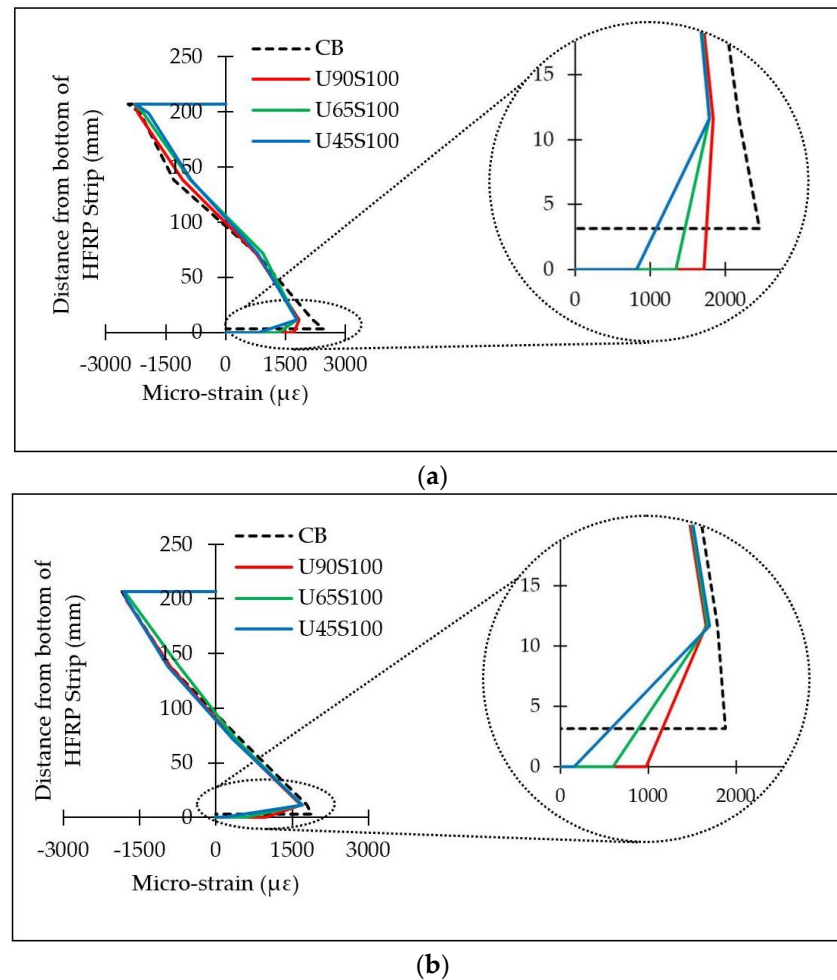


Figure 11. Strain profiles of CB, U90S100, U65S100, and U45S100 at: (a) mid-segment and (b) edge-segment at 310 kN.

Table 3. Percentage utilization of the ultimate strength of the bolted HFRP strips at 310 kN.

Specimen Designation	ϵ_{HFRP} at Mid-Segment ($\mu\epsilon$)	$U_{\sigma\text{HFRP}}$ at Mid-Segment (%)	ϵ_{HFRP} at Edge-Segment ($\mu\epsilon$)	$U_{\sigma\text{HFRP}}$ at Edge-Segment (%)
U90S100	1716	12.5	980	7.2
U65S100	1340	9.8	598	4.4
U45S100	815	5.9	160	1.2
U90D35	2154	15.7	1576	11.5
U65D35	2148	15.7	1239	9.0
U45D35	1192	8.7	179	1.3
ST90S100	1899	13.9	1348	9.8
ST65S100	1300	9.5	510	3.7
ST45S100	665	4.9	9	0.1
ST90D35	2376	17.3	1647	12.0

Comparing the tensile strains in the HFRP strips to those at the bottom steel flange reflects the relative slippage experienced by each configuration at the HFRP–steel interface. Increasing the HFRP length significantly reduced the slippage between the bolted components and enhanced the sectional strain compatibility. The calculated difference in the

tensile strains between the HFRP and the steel flange in U90S100 was $125 \mu\epsilon$, compared to $976 \mu\epsilon$ in U45S100, indicating an 87.2% reduction in the slippage in the mid-segment at 310 kN. Similarly, the strain profiles of U90D35 and U65D35 at 310 kN showed better strain compatibility and lower interfacial slippage than that of U45D35 in both segments (see Figure 12). The measured strains in the bottom steel flange of U90D35 were lower than those of CB, U45D35, and U65D35 by 25.4%, 18.4%, and 17.6%, respectively. The effectiveness of the long HFRP strips in reducing the tensile strains in the strengthened beams was also noticeable in the beams fastened by steel bolts in staggered arrangements, as shown in Figure 13 and by the $\%U_{\sigma_{\text{HFRP}}}$ in Table 3.

The distributions of the flexural strains along the span of the HFRP strip of U90S100, U65S100, and U45S100 at 380 kN are displayed in Figure 14. It should be noted that the strain gauges instrumented only half the span of the tested beams; however, the symmetry maintained in the beam geometry and the loading conditions enabled the mirroring of the recorded strains over the beam centerline to provide a better presentation of the strains along the full length of the bolted HFRP strips. The plotted flexural strains showed a similar trend to that of the distribution of the bending moment diagram of a simply supported beam subjected to four-point loading with minor disturbances. This agrees with the reported findings for bonded FRP–steel beams [38–41]. The plotted disturbances can be attributed to the effects of the random distribution of the glass fibers within the HFRP strip. Figure 14 shows a better contribution of the long HFRP in resisting the applied loads, as is made evident by the higher strain measurements along U90S100 compared to those recorded in U65S100 and U45S100 at any specific distance from the beam centerline.

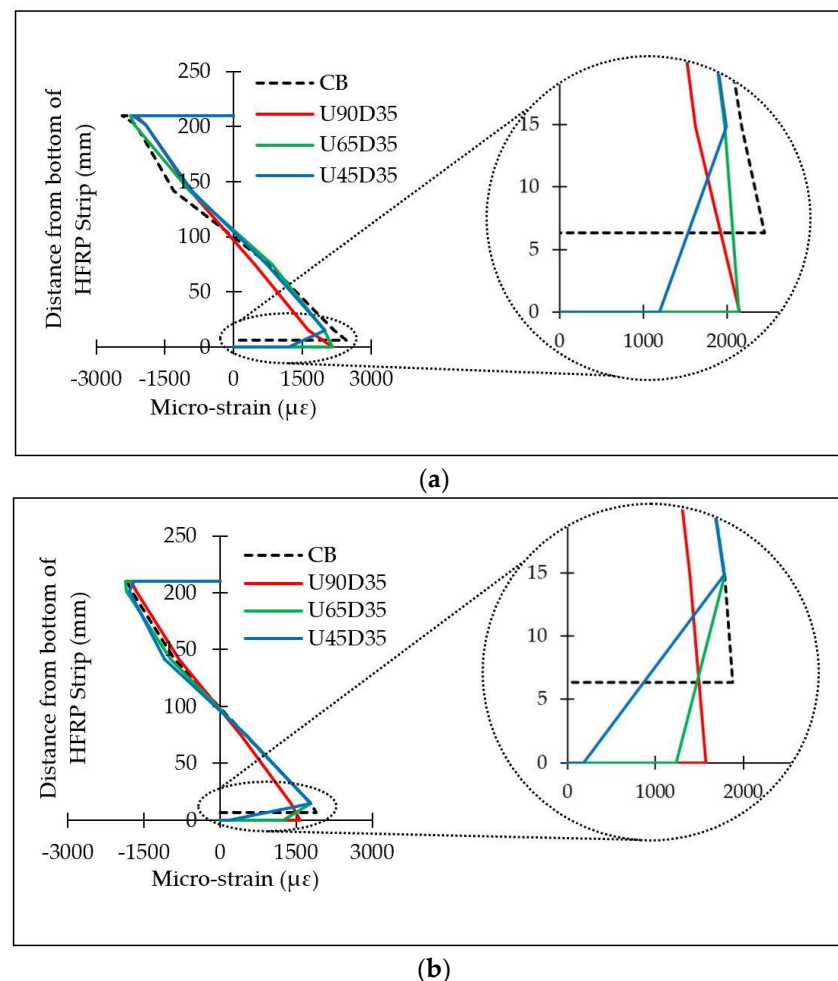
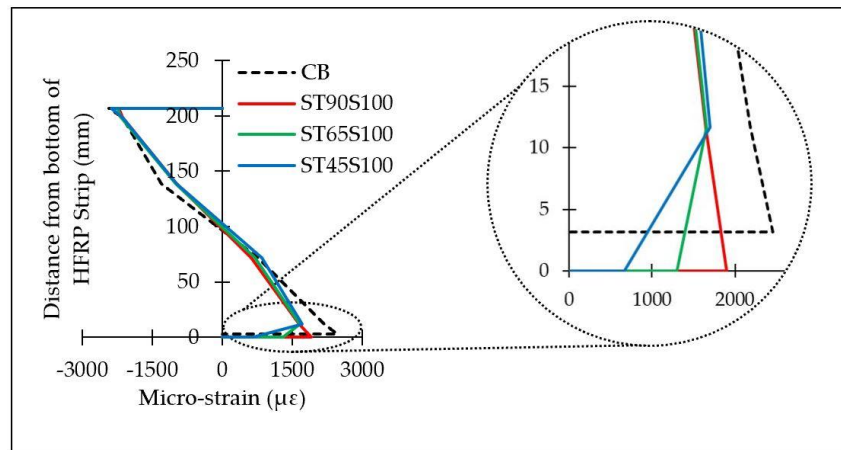
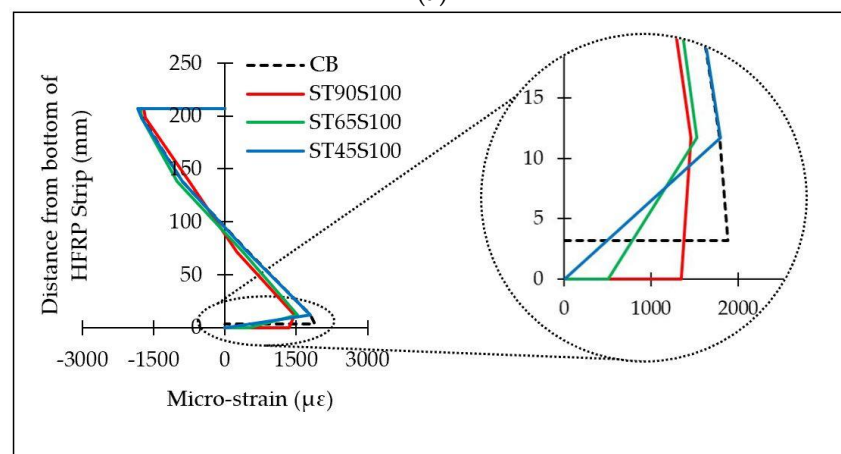


Figure 12. Strain profiles of CB, U90D35, U65D35 and U45D35 at: (a) mid-segment and (b) edge-segment at 310 kN.



(a)



(b)

Figure 13. Strain profiles of CB, ST90S100, ST65S100, and ST45S100 at: (a) mid-segment and (b) edge-segment at 310 kN.

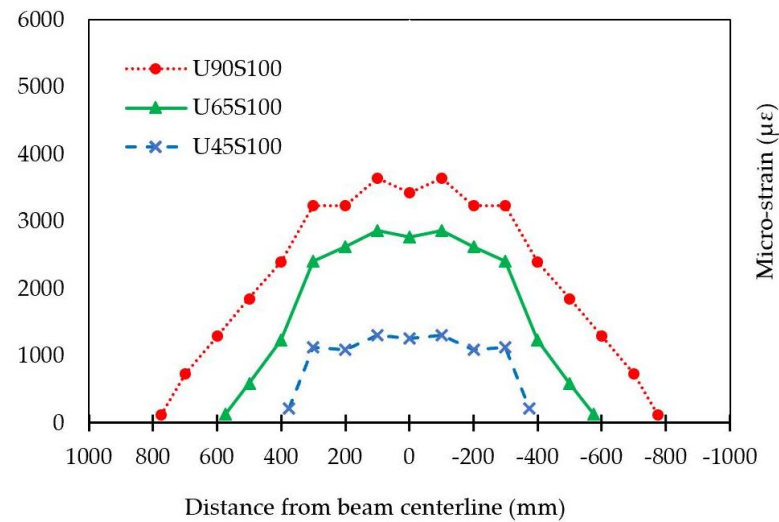


Figure 14. Strain distribution along the HFRP strips of U90S100, U65S100, and U45S100 at 380 kN.

3.3. Effect of Bolt Arrangement

Analyzing the effect of the bolt arrangement was conducted by coupling the configurations that exhibited similar fastening parameters except for the bolt arrangement. The results of U90S100 and ST90S100 were compared to evaluate the effects of the bolt

arrangement while using a single 1620 mm long HFRP strip. Similarly, specimen pairs (U65S100 and ST65S100) and (U45S100 and ST45S100) were compared for the shorter HFRP strips. In addition, the experimental performance of U90D35 and ST90D35 was compared to assess the effect of the bolt arrangement while using double HFRP strips.

3.3.1. Load-Deflection Curves

The load-deflection curves of the aforementioned configuration pairs are displayed in Figure 15. The beams strengthened with staggered bolts showed similar elastic and plastic performances to the beams strengthened with uniform bolts. This insignificant difference between using uniform and staggered bolt arrangements may be attributed to having the same number of bolts in both configurations, in addition to the small gauge line distance of 15 mm in the staggered configuration enforced by the small width of the beam's flange.

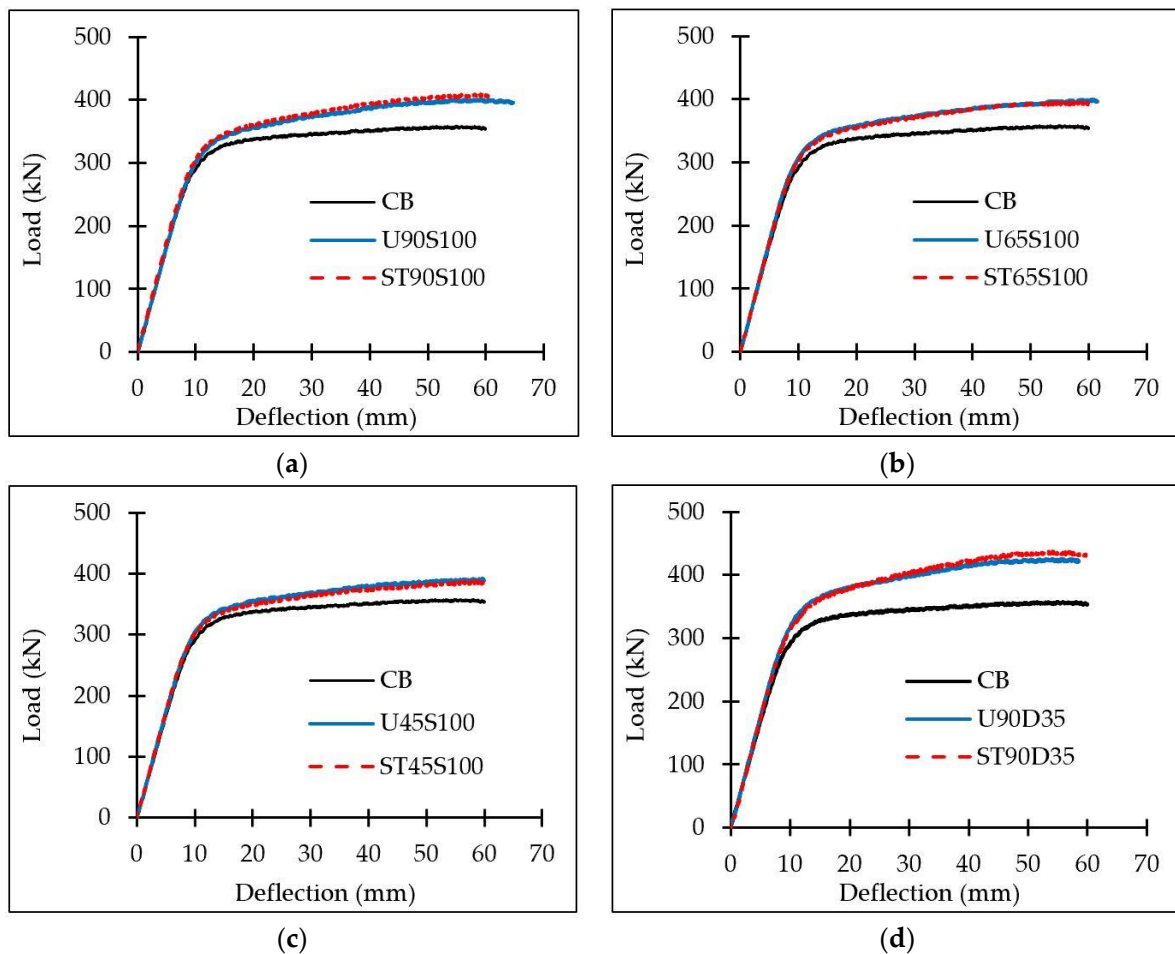


Figure 15. Load-deflection curves of the configuration pairs with uniform and staggered bolts: (a) U90S100 and ST90S100; (b) U65S100 and ST65S100; (c) U45S100 and ST45S100; (d) U90D35 and ST90D35.

3.3.2. Strain Measurements

Figure 16 displays the strain profiles at the mid-segments of the configuration pairs at 310 kN. Although ST90S100 showed slightly better compatibility and lower slippage than U90S100, the remaining specimens showed that the bolt arrangement had an insignificant effect on the strain distribution. Comparing the $\%U_{\sigma_{\text{HFRP}}}$ of the configuration pairs in Table 3 indicates a similar utilization of the HFRP strip regardless of the bolt arrangement in both segments.

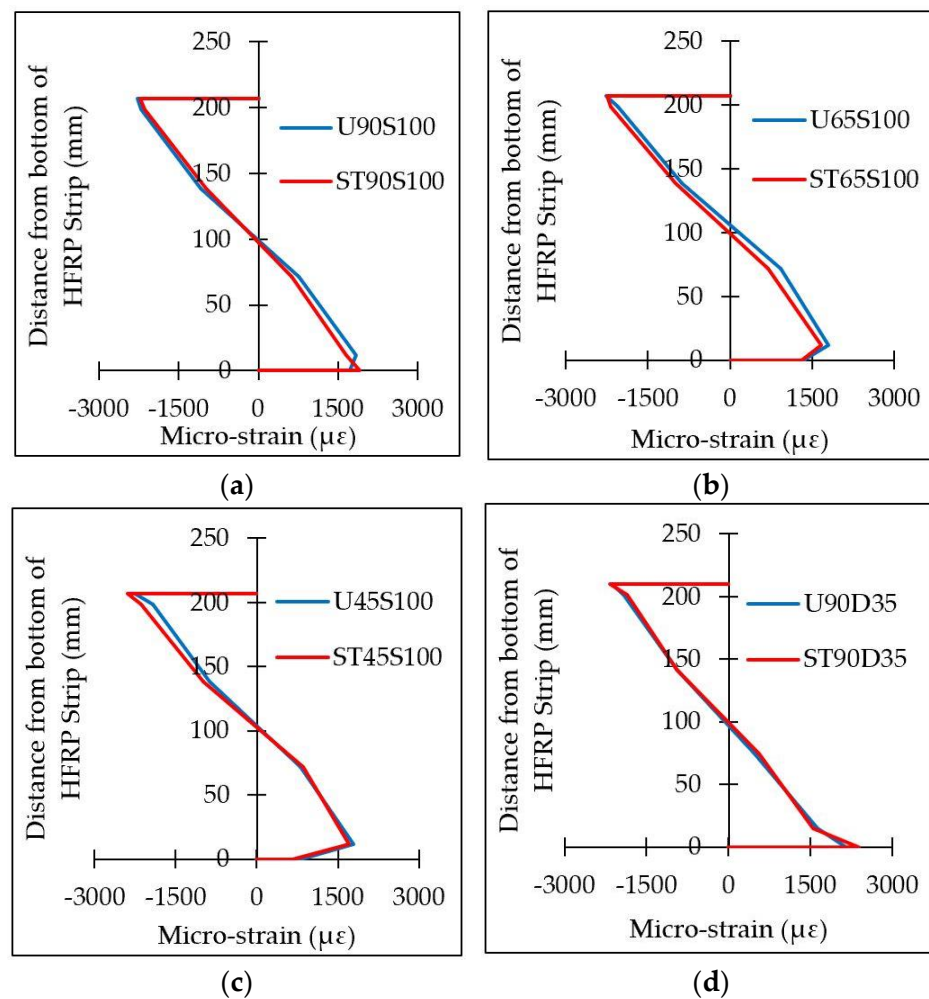


Figure 16. Strain profiles at the mid-segments of the configuration pairs with uniform and staggered bolts: (a) U90S100 and ST90S100; (b) U65S100 and ST65S100; (c) U45S100 and ST45S100; (d) U90D35 and ST90D35.

3.4. Development of Empirical Load-Deflection Equations

Simplified empirical equations characterizing the load-deflection relation of the strengthened beams were developed based on the experimental records discussed in Section 3. The proposed equations are presented in a normalized form where the ordinate is calculated by dividing the experimental load by the ultimate load of the respective configuration (P/P_u). Meanwhile, the abscissa is presented by dividing the recorded deflections by the beam clear span (δ/L_{clear}), where L_{clear} equals 1800 mm. The corresponding generalized curves are shown in Figure 17 for sample configurations. These plots are characterized by three distinct zones, namely the linear elastic zone that extends till the onset of yielding at $\delta/L_{clear} = 0.005$ (zone A); the plastic zone (zone C) that corresponds to $\delta/L_{clear} \geq 0.01$; and the transitional zone (zone B) between the two former zones where propagation of the yielding takes effect. The values of the normalized ordinates (P/P_u) along with the corresponding abscissas (δ/L_{clear}) for all the specimens were incorporated into MATLAB to generate empirical equations that best fit all three zones, resulting in the following:

$$P/P_u = 147 \left(\delta/L_{clear} \right), \text{ for } \left(\delta/L_{clear} \right) \leq 0.005 \quad (2)$$

$$P/P_u = -5560 \left(\delta/L_{clear} \right)^2 + 116 \left(\delta/L_{clear} \right) + 0.277, \text{ for } 0.005 \leq \left(\delta/L_{clear} \right) \leq 0.01 \quad (3)$$

$$P/P_u = -195 \left(\delta/L_{clear} \right)^2 + 13.5 \left(\delta/L_{clear} \right) + 0.759, \text{ for } 0.01 \leq \left(\delta/L_{clear} \right) \quad (4)$$

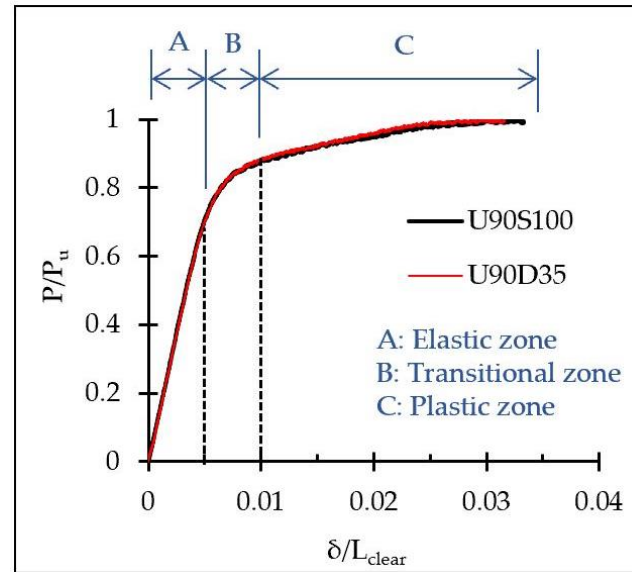


Figure 17. Generalized curves for specimens U90S100 and U90D35.

Another round of regression analysis was conducted using the data points of all the tested specimens to enable the prediction of the ultimate load of a bolted HFRP–steel beam as a function of the length of the HFRP strip (L_{HFRP}), the clear span of the beam (L_{clear}), the spacing between the steel bolts (S), and the hole diameter (D), as follows:

$$P_u = \left(\alpha^2 / 4\beta \right) + \gamma \quad (5)$$

$$\alpha = 1.8 + 2.787 \left(L_{HFRP} / L_{clear} \right) - 0.089 \left(S / D \right) \quad (6)$$

$$\beta = 0.0079 + 0.0294 \left(L_{HFRP} / L_{clear} \right) - 0.0007 \left(S / D \right) \quad (7)$$

$$\gamma = 318.8 - 20.7 \left(L_{HFRP} / L_{clear} \right) + 0.634 \left(S / D \right) \quad (8)$$

where (P_u) is the ultimate load of the strengthened system in kN, (L_{HFRP}) is the length of the HFRP strip in mm, (L_{clear}) is the clear span of the beam in mm, (S) is the spacing between the steel bolts in mm, and (D) is the diameter of the bolt hole in mm, which is 2 mm larger than the bolt diameter. It is worth noting that the arrangement of the steel bolts was not incorporated in the empirical equations due to its negligible effect on the ultimate load of the strengthened beams, as discussed in Section 3.3. Similarly, the thickness of the HFRP was not integrated into the proposed equations due to its insignificant influence, as reported in [34]. Table 4 shows a comparison between the experimental and empirical ultimate loads, with a maximum difference of less than 2% with the exception of the U45D35 specimen, which had an error of 5.7%. The adequacy of the proposed empirical equations was further validated against the experimental measurements of all the tested specimens, as shown in Figure 18. The plotted curves confirm the good agreement between the experimental and the empirically predicted load-deflection curves.

Table 4. Experimental and empirical ultimate loads.

Specimen Designation	$P_{u,EXP}$ ^{*a} (kN)	$P_{u,EMP}$ ^{*b} (kN)	Error (%)
U90S100	400.38	407.79	1.9
U65S100	399.31	398.77	0.1
U45S100	392.5	393.54	0.3
U90D35	425.37	425.62	0.1
U65D35	411.86	416.51	1.1
U45D35	388.31	410.52	5.7
ST90S100	408.92	407.79	0.3
ST65S100	395.93	398.77	0.7
ST45S100	388.44	393.54	1.3
ST90D35	437.52	425.62	2.7

^{*a}: Experimental load; ^{*b}: Empirical load.

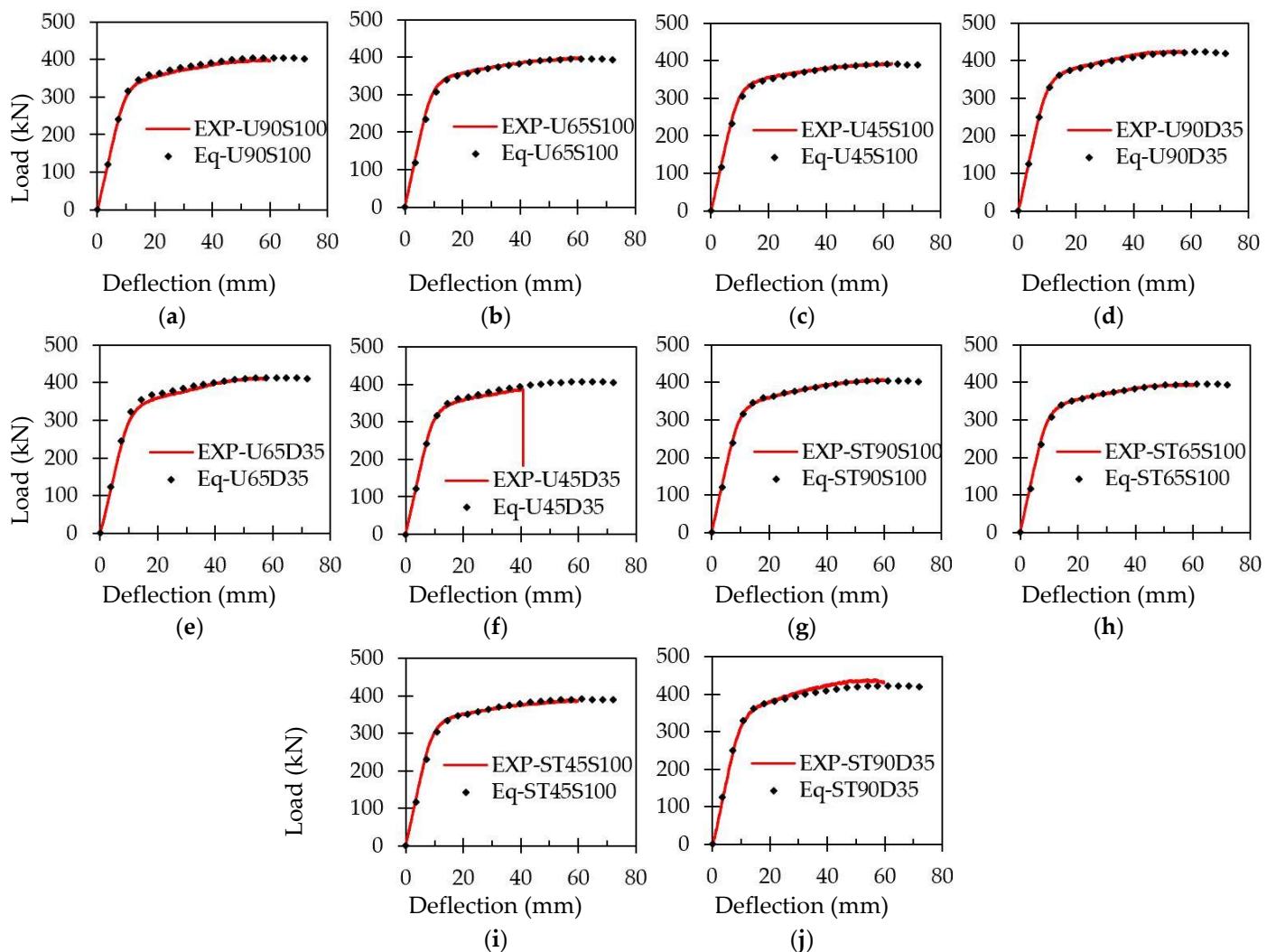


Figure 18. Experimental and empirical load-deflection curves of beams fastened by steel bolts: (a) U90S100; (b) U65S100; (c) U45S100; (d) U90D35; (e) U65D35; (f) U45D35; (g) ST90S100; (h) ST65S100; (i) ST45S100; (j) ST90D35.

4. Finite Element Modeling

A detailed three-dimensional (3D) numerical model was developed using the multi-purpose finite element (FE) software ANSYS (2020 R1) [42] to simulate the performance of

the strengthened HFRP–steel beams. Detailed descriptions of the model geometry, material modeling, and boundary conditions are outlined hereafter. The accuracy of the developed FE model was verified by comparing the load-deflection curves, deflection profiles, and failure modes of all the tested specimens with their counterparts from the finite element model. Finally, a parametric numerical study was conducted using the verified model to assess the effectiveness of the fastening technique when considering a wide range of parameters, including HFRP thickness, bolt spacing, steel grade, loading scheme, and beam length.

4.1. Model Development

4.1.1. Description and Geometry

Geometrical and material nonlinearities were considered in the modeling of the various components of the HFRP–steel system. The steel beams, stiffeners, HFRP strips, and spreader beam were modeled using the 3D 8-node structural element SOLID185, which incorporates plasticity, stress stiffening, large deflection, and large strain capabilities. Meanwhile, the HFRP–steel connectivity was modeled using the unidirectional nonlinear spring element COMBIN39. The nonlinear force-deflection capability of the COMBIN39 enabled the simulation of the interfacial behavior at the HFRP–steel interface by incorporating the load-slip model proposed by Abou El-Hamd et al. [27], as shown in Figure 19. The adopted load-slip model accounts for the various interactions taking place at the HFRP–steel interface. It is worth noting that the incorporated load-slip model was developed for HFRP–steel joints fastened by M6 steel bolts that are identical to those presented in Section 2.1. The COMBIN39 element was used to connect two coincident node points: one of which was located on the bottom steel flange and the other was placed at the inner surface of the HFRP strip. The modeled spreader beam was also connected to the tested steel beam at the locations of the two loading points using the COMBIN39 element. The COMBIN39 element was defined in the three basic directions (X, Y, and Z) to simulate the spatial connectivity between the fastened components.

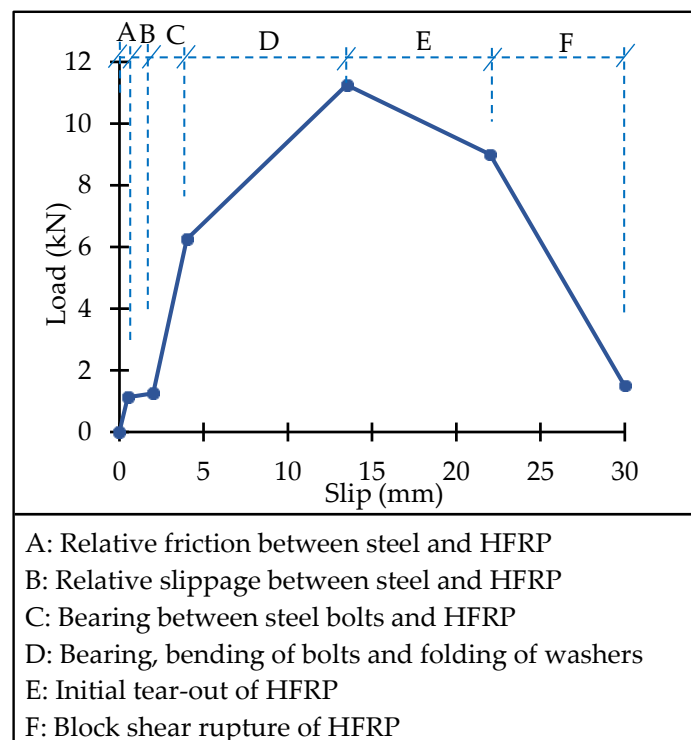


Figure 19. Load-slip model for HFRP–steel fastened joints using M6 steel bolt [27].

The general geometry of the modeled HFRP–steel beam with the spreader is shown in Figure 20. The geometry was defined using a global Cartesian coordinate system with its origin located at the external surface of the bottom steel flange at the beam’s mid-span. The beam depth was directed along the Y-axis, while its span was parallel to the Z-axis. The main geometrical parameters of the beam were its length (L), clear span (L_{clear}), flange thickness (t_f), flange width (b_f), web thickness (t_w), and web height (h_w). Additionally, 12 mm thick endplates and stiffeners were modeled at the locations described in Section 2. Meanwhile, the geometry of the modeled HFRP strip was defined by its width (b_{HFRP}), thickness (t_{HFRP}), and length (L_{HFRP}). The COMBIN39 element was introduced at the bolt locations to model the connectivity between the steel beam and the HFRP (see Figure 21). The COMBIN39 element was defined by stiff springs in the X- and Y-directions to simulate the zero-loading in the X-direction and to reflect the restrictions imposed by the clamping forces in the Y-direction. Meanwhile, the interfacial behavior at the HFRP–steel interface was modeled using the non-linear COMBIN39 spring directed in the Z-direction with a profile that matches the load-slip model shown in Figure 19.

The spreader beam was modeled as a solid component with length ($L_{spreader}$), width ($b_{spreader}$) and height ($h_{spreader}$) matching those of the spreader utilized in the experimental testing (refer to Figure 20). A significantly stiff COMBIN39 element was defined in the Y-direction to connect the bottom surface of the spreader beam to the upper surface of the top steel flange at the loading locations and defined as “Loading Nodes”. A sensitivity analysis was performed to simulate the experienced friction between the spreader and the strengthened steel beam. The results were incorporated into the spreader’s COMBIN39 element in the X-direction and Z-direction.

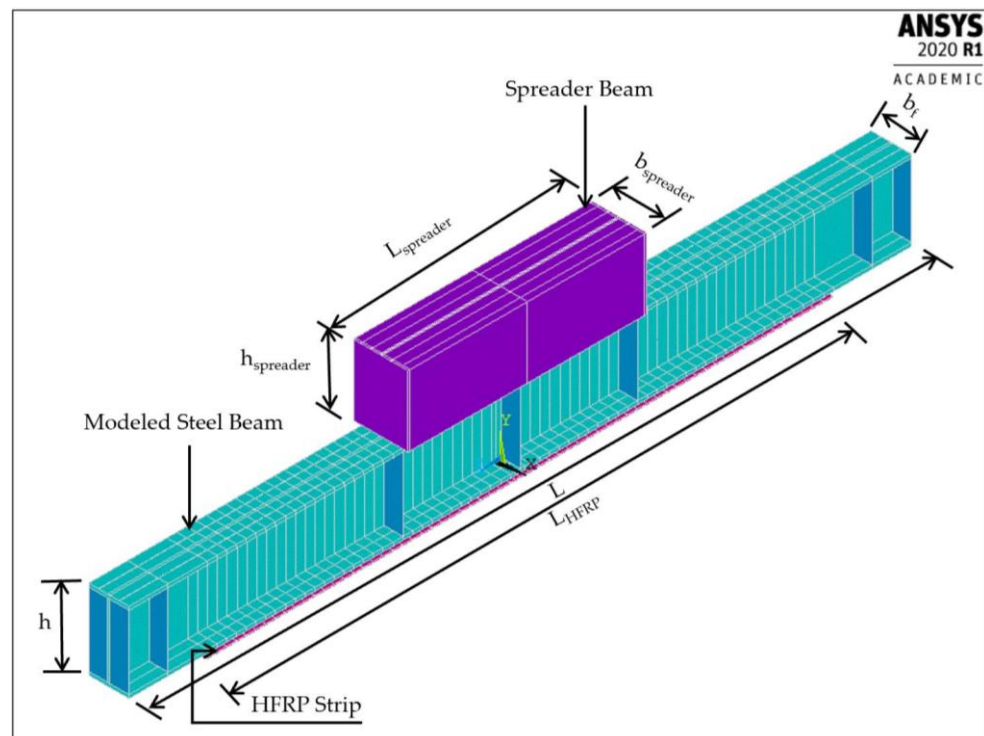


Figure 20. General geometry of the modeled HFRP–steel beam.

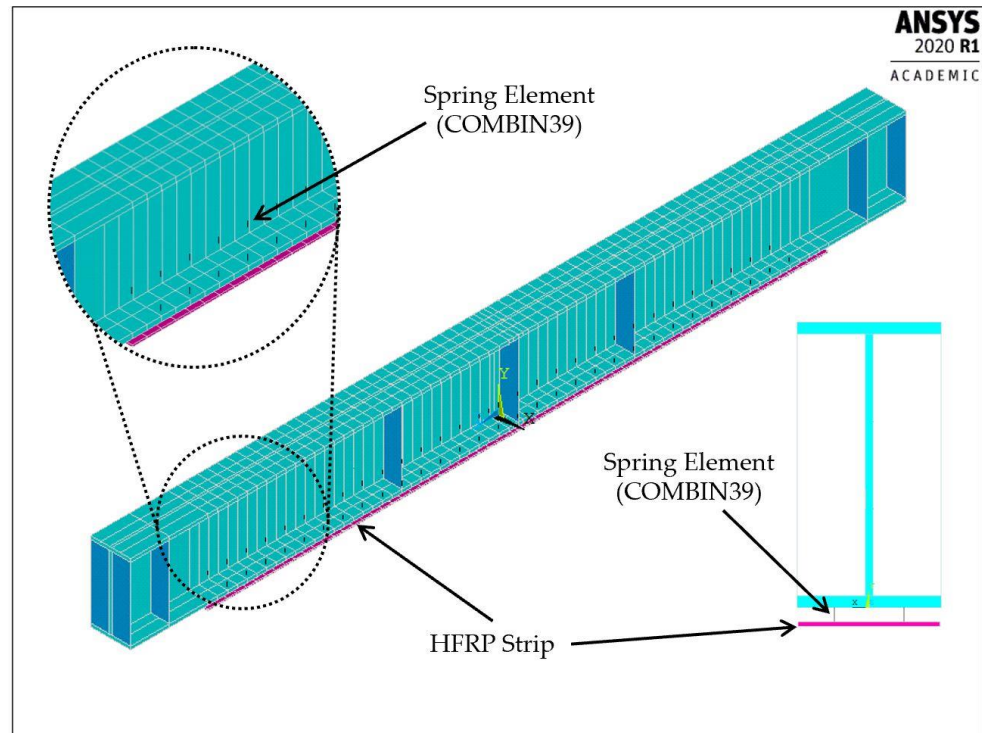


Figure 21. Locations of the steel bolts (COMBIN39) in the modeled U90S100 beam (spacing between the bottom steel flange and HFRP is exaggerated for clarity of the presentation).

4.1.2. Material Modeling

The multi-linear stress-strain curve proposed by Salmon et al. [43] was used to model the steel material, as shown in Figure 22. The described material model has an elastic Young's modulus E of 180,000 MPa, a yield stress σ_y of 465 MPa, an ultimate stress σ_u of 620 MPa, and a Poisson's ratio ν of 0.3. The steel tangential modulus E_t was set to a value of 1.5% E (2700 MPa), as depicted in the revised material model proposed by Foster et al. [44].

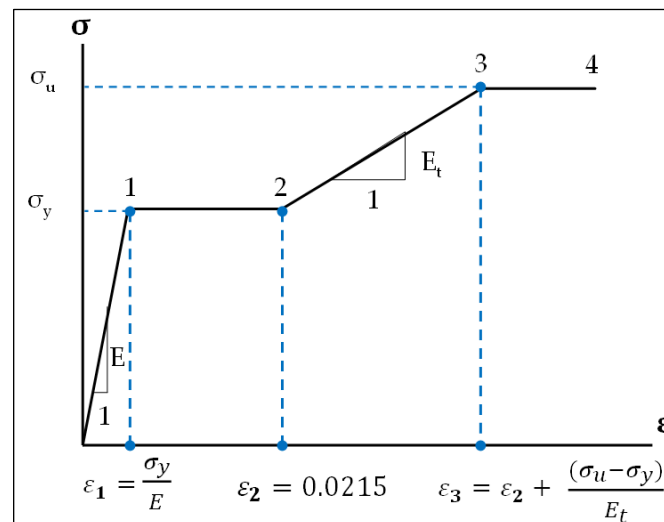


Figure 22. Stress-strain curve for modeling the mechanical properties of the steel material.

The HFRP strips were modeled as a linear elastic material with a longitudinal elastic modulus E_z of 62,190 MPa, as reported in the manufacturer's datasheet. Meanwhile, the transverse elastic moduli of the HFRP strips, E_y and E_x , were taken as 4800 MPa [45]. The Poisson's ratios ν_{yx} , ν_{zx} , and ν_{yz} were equal to 0.30, 0.22, and 0.22, respectively [45,46].

4.1.3. Boundary Conditions

The displacements in the X-direction (U_x) and Y-direction (U_y) at the bottom steel flange were restricted to model the beam supports, as shown in Figure 23. In order to enforce the symmetry conditions in the Z-direction, the longitudinal displacement (U_z) at the mid-span node was restrained. The effect of the lateral braces on the spreader beam was embedded by restraining the top nodes of the spreader at both ends in the X-direction (U_x). Meanwhile, all the other nodes of the model were left unrestrained against any translation. It should be noted that the numerical analysis was conducted in a displacement-controlled manner in the Y-direction. The numerical simulations were terminated following the adoption of the same principle in the experimental testing of the beams. This implies a termination deflection of 60 mm or the occurrence of the shear fracture of the steel bolts.

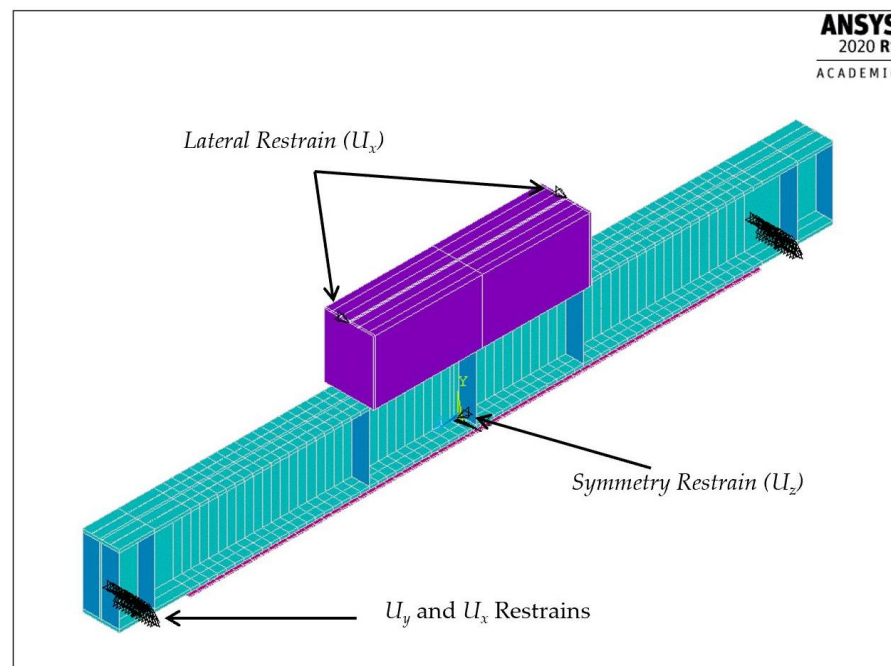


Figure 23. Boundary conditions of the modeled HFRP–steel beam.

4.2. Model Verification

The validation process was carried out by comparing the numerical predictions to the experimental measurements of all the tested beams. The experimental and numerical load-deflection curves of the modeled configurations are displayed in Figure 24. It is worth noting that the model was capable of predicting the bolt shear fracture experienced by U45D35 (see Figure 8), as reflected in the load drop displayed in Figure 24g. According to the experimental observations, bolt failure took place at a load of 375.5 kN and a deflection of 34.77 mm at the exterior bolt. The numerically retrieved bolt force at the failed bolt was 11.03 kN, exceeding the 10.6 kN shear capacity of the $M6 \times 40$ bolt. The excellent match between the experimental curves and the numerical predictions of the tested configurations verifies the ability of the model to accurately predict the response of the bolted HFRP–steel systems at various loading stages. In addition, the model predicted the experimentally observed failure modes (LTB and FLB), as shown in Figure 25. The experimental and numerical yield loads and ultimate loads of the modeled beams are reported in Table 5. The percentage difference between the experimental and numerical yield loads ranged from 0.05% to 2.95%, while that of the ultimate loads ranged between 0.07% and 10.22%, indicating excellent agreement between the test records and the numerical values. For further verification, the experimental and numerical deflection profiles of all the specimens were plotted and are compared in Figure 26. It is noteworthy that the deflection profiles plotted in the figure correspond to loads of 200 kN, 300 kN, and 350 kN for the beams strengthened by a single HFRP strip. Meanwhile, the experimental and numerical deflection

profiles of the configurations with double HFRP strips were plotted at 200 kN, 310 kN, and 360 kN. The differences between the experimental and numerical mid-span deflections at 350 kN and 360 kN are presented in Table 6 with an error range of 0.3% to 13.85%. As is evident in Figure 26, the differences between the experimental and numerical deflection profiles at all other load values are considerably less than those reported in Table 6.

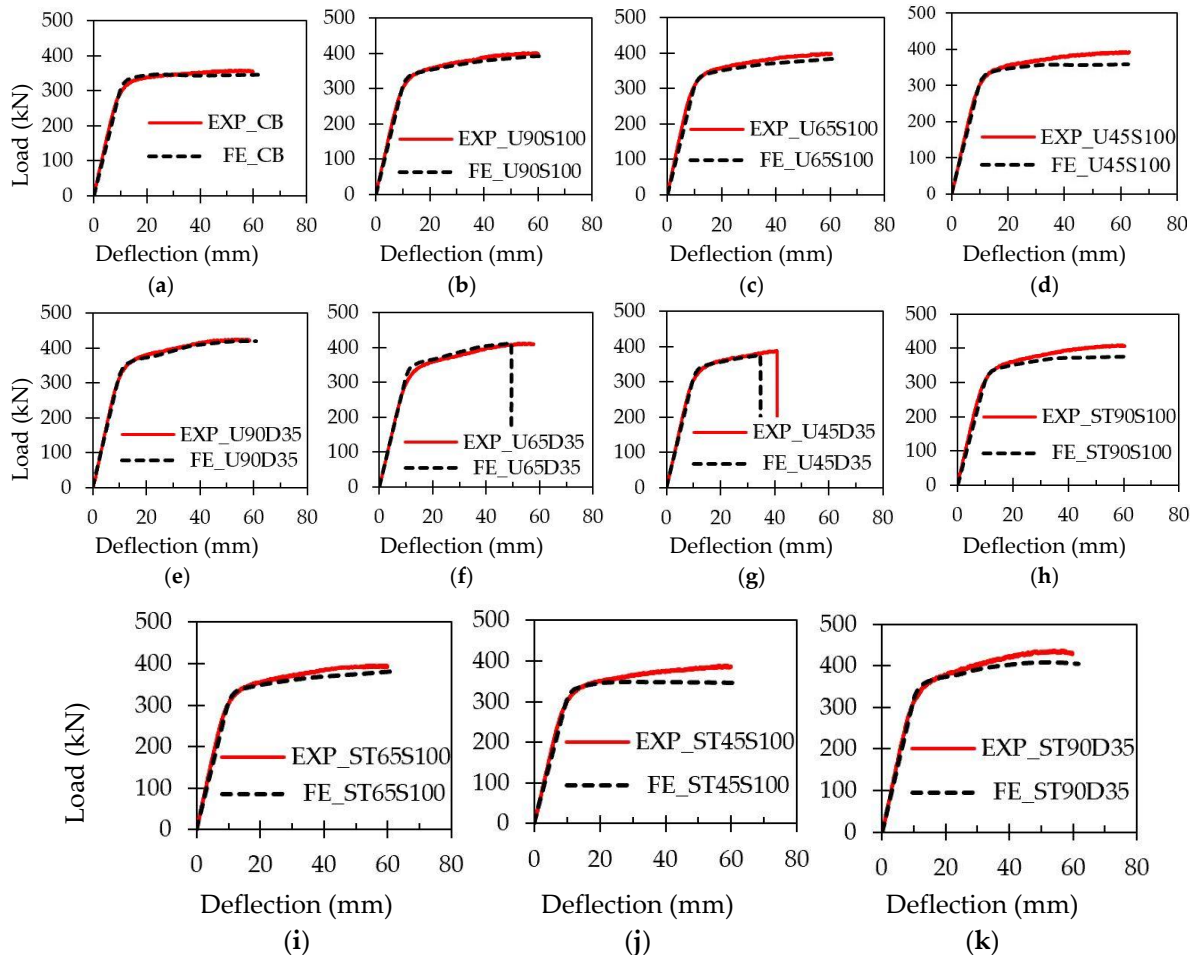


Figure 24. Experimental and numerical load-deflection curves of the modeled beams: (a) CB; (b) U90S100; (c) U65S100; (d) U45S100; (e) U90D35; (f) U65D35; (g) U45D35; (h) ST90S100; (i) ST65S100; (j) ST45S100; (k) ST90D35.

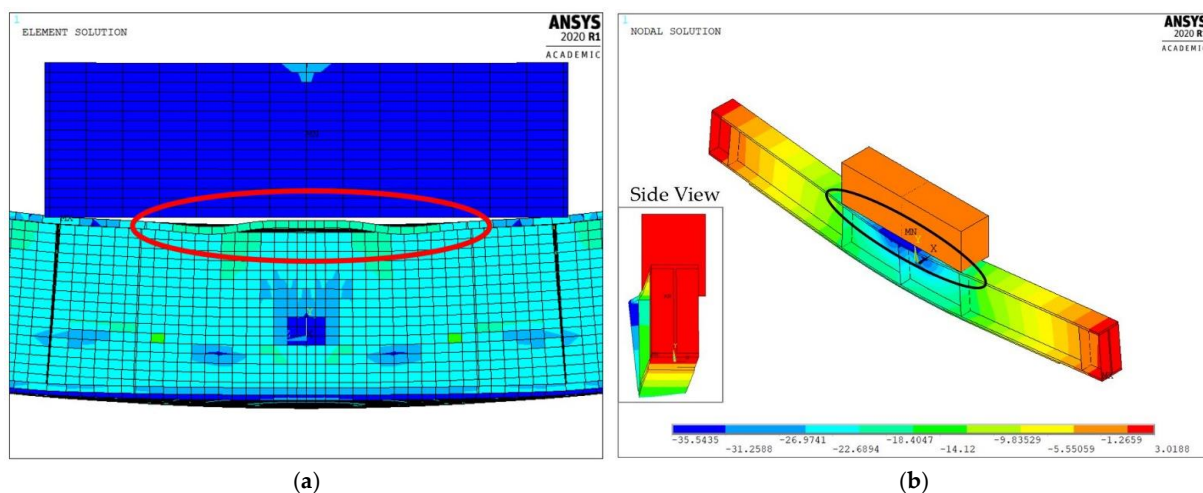


Figure 25. Numerical behavior of U90D35: (a) FLB; (b) lateral deflection and LTB.

Table 5. Experimental and numerical yield loads and ultimate loads of the modeled beams.

Specimen Designation	Yield Load (kN)			Ultimate Load (kN)		
	$P_{y,EXP}$ ^{*a} (kN)	$P_{y,FE}$ ^{*b} (kN)	ΔP_y (%)	$P_{u,EXP}$ ^{*a} (kN)	$P_{u,FE}$ ^{*b} (kN)	ΔP_u (%)
CB	260.79	258.86	0.74	358.01	346.45	3.23
U90S100	283.15	277.56	1.97	400.38	390.54	2.46
U65S100	275.84	276.11	0.10	399.31	381.91	4.36
U45S100	273.47	274.85	0.50	392.50	358.46	8.67
U90D35	300.10	296.36	1.25	425.37	420.52	1.14
U65D35	288.71	285.30	1.18	411.86	412.15	0.07
U45D35	287.71	279.21	2.95	388.31	375.48	3.30
ST90S100	282.96	276.87	2.15	408.92	375.69	8.13
ST65S100	280.46	275.46	1.78	395.93	381.68	3.60
ST45S100	274.41	274.27	0.05	388.44	348.76	10.22
ST90D35	292.77	290.13	0.90	437.52	408.39	6.66

^{*a}: Experimental load; ^{*b}: Finite element (numerical) load.

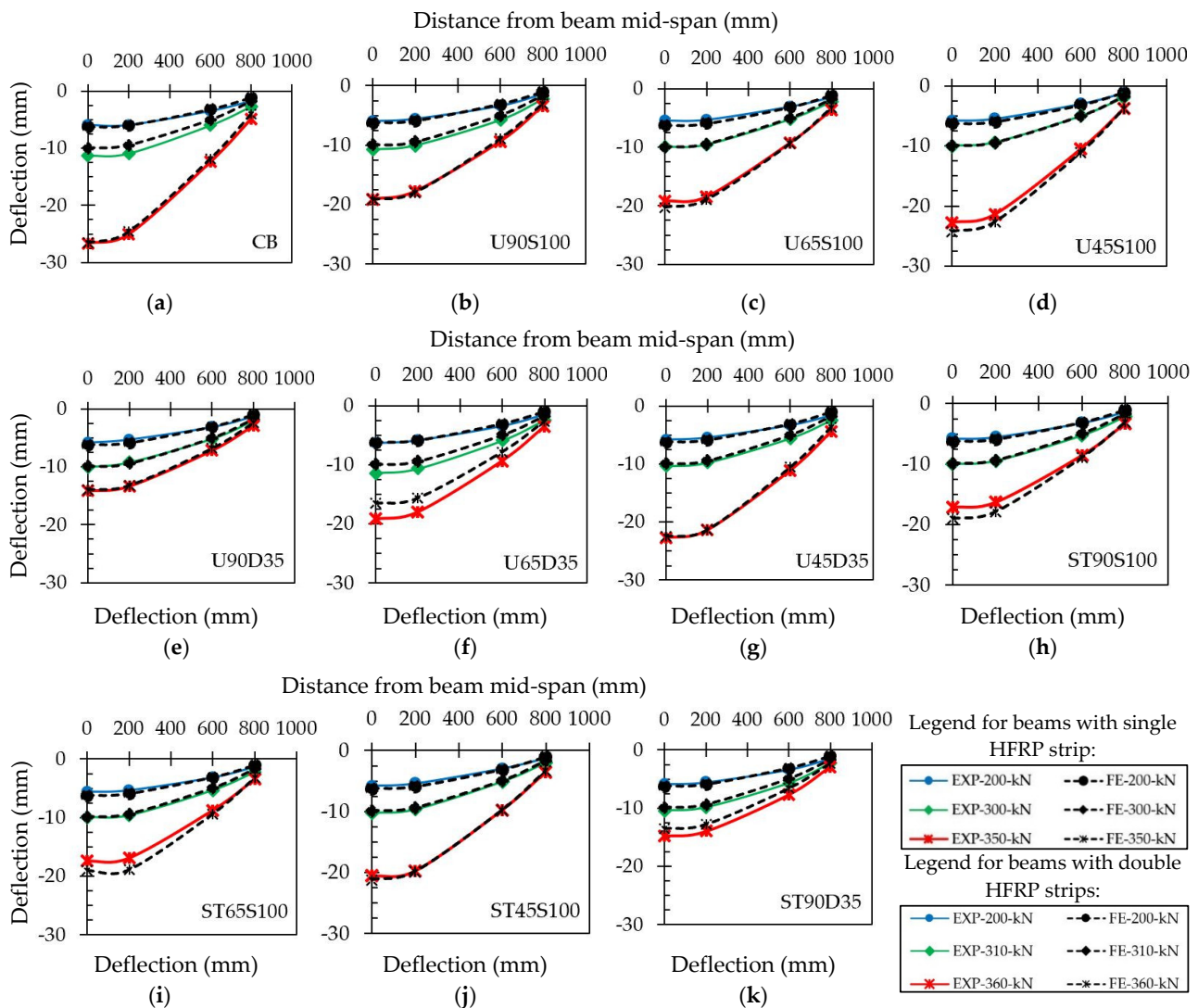


Figure 26. Experimental and numerical deflection profiles of the modeled beams: (a) CB; (b) U90S100; (c) U65S100; (d) U45S100; (e) U90D35; (f) U65D35; (g) U45D35; (h) ST90S100; (i) ST65S100; (j) ST45S100; (k) ST90D35.

Table 6. Experimental and numerical mid-span deflections of the modeled beams.

Specimen Designation	Mid-Span Deflection at Load of 350 kN for Single HFRP and Load of 360 kN for Double HFRP		Error (%)
	D _{EXP} (mm) ^{*a}	D _{FE} (mm) ^{*b}	
CB	−26.66	−26.58	0.30
U90S100 ^{*c}	−19.10	−19.16	0.31
U65S100 ^{*c}	−19.19	−20.29	5.73
U45S100 ^{*c}	−22.75	−24.27	6.68
U90D35 ^{*d}	−14.15	−13.98	1.20
U65D35 ^{*d}	−19.14	−16.49	13.85
U45D35 ^{*d}	−22.73	−22.51	0.97
ST90S100 ^{*c}	−17.14	−19.02	10.97
ST65S100 ^{*c}	−17.40	−19.02	9.31
ST45S100 ^{*c}	−20.55	−21.18	3.07
ST90D35 ^{*d}	−14.76	−13.47	8.74

^{*a}: Experimental deflection at mid-span; ^{*b}: Finite element (numerical) deflection at mid-span; ^{*c}: Configurations with single HFRP strip (i.e., reported mid-span deflection is at 350 kN); ^{*d}: Configurations with double HFRP strips (i.e., reported mid-span deflection is at 360 kN).

4.3. Parametric Finite Element Study

The verified FE model was used to conduct a parametric study on steel beams strengthened by fastening HFRP strips at the tension flange. All the modeled beams in the parametric study were strengthened with an HFRP length that was 90% of the beam clear span and fastened by steel bolts in uniform arrangements.

The FE models of beams U90S100 and U90D35 were used as a baseline to conduct the parametric study; therefore, the effect of the parameters was examined considering the two spacing values tested experimentally (i.e., 100 mm and 35 mm). The parametric study was divided into four sets depending on the variable parameter of interest (targeted parameter). The first set of models was used as a reference and named the “reference set”, in which the effect of the HFRP thickness and the spacing between the bolts for beams made of G60 steel with 1800 mm clear span and subjected to four-point loading (4PL) was examined. Afterwards, only the targeted parameter was changed, and its effect was compared to the reference set. The designation of each FE model in this section consists of four symbols describing the main fastening parameters in the form of “A-B-C-D”. Table 7 relates each symbol in the designation to the examined parameter and the modeled levels of each parameter. The number in the first symbol denotes the number of the HFRP strips, while the “PL” at the “C” symbol stands for the “point loading”. For example, model 2HFRP-A36-4PL-S100 reflects the numerical performance of a beam made of A36 steel, strengthened by two HFRP strips using steel bolts spaced at 100 mm and subjected to four-point loading (4PL). The following subsections describe the modifications in the finite element model to enable the examination of the targeted parameter along with the numerical results of each set.

Table 7. Designation of the FE models in the parametric study.

Symbol	Examined Parameter	Examined Levels
A	HFRP thickness	1HFRP, 2HFRP, 4HFRP
B	Steel grade	G60, A36
C	Loading scheme	4PL, 3PL
D	Spacing between bolts	100 mm, 35 mm

4.3.1. HFRP Thickness and Bolt Spacing

The verified FE model of the U90S100 beam in Section 4.2 represents the performance of a steel beam made of G60 steel and strengthened by one HFRP strip (1HFRP) fastened

by steel bolts spaced at 100 mm and subjected to 4PL. According to Table 7, the designation of this beam is 1HFRP-G60-4PL-S100. To examine the effect of the HFRP thickness on the performance of the strengthened beam, two FE models were developed with two and four layers of the HFRP strips, representing HFRP thicknesses of 6.35 mm and 12.7 mm, respectively, while maintaining 100 mm spacing between the bolts. Similarly, the verified FE model of the U90D35 beam described in Section 4.2 provides the performance of the 2HFRP-G60-4PL-S35 model. Two additional finite element models were developed to simulate the behavior of similar beams strengthened by one and four HFRP strips.

Comparing the numerical performance of 1HFRP-G60-4PL-S100, 2HFRP-G60-4PL-S100, and 4HFRP-G60-4PL-S100 in Figure 27 reflects the effect of the HFRP thickness while keeping the 100 mm spacing between the bolts unchanged. Increasing the thickness of the HFRP strip by utilizing two and four HFRP strips slightly improved the yield load of the system, as shown in Figure 27b. Meanwhile, increasing the HFRP thickness reduced the ultimate load-carrying capacity and ductility of the strengthened beam due to the failure of the bolts. The shear failure of the bolts was reflected by a sudden drop in the load-deflection curves, as shown for the 2HFRP-G60-4PL-S100 and 4HFRP-G60-4PL-S100 models. Configuration 1HFRP-G60-4PL-S100 showed the best performance in terms of ductility and ultimate load-carrying capacity for the considered fastening conditions.

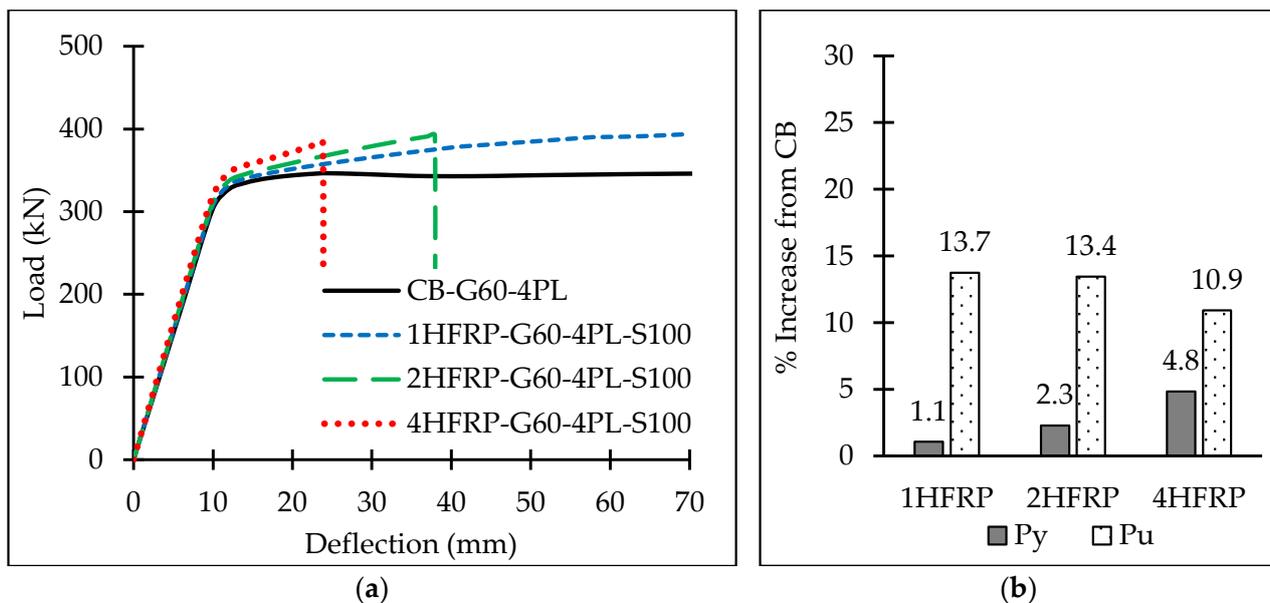


Figure 27. Effect of HFRP thickness with 100 mm spacing in G60 steel beams: (a) load-deflection curves; (b) % increase in yield and ultimate loads from CB.

Reducing the spacing between the bolts from 100 mm to 35 mm enhanced the yield and ultimate load capacities of the beam. The 4HFRP-G60-4PL-S35 model showed 10.4% and 25.2% improvements in the yield and ultimate loads, respectively, compared to the CB, as shown in Figure 28b. However, the ductility of the beam was reduced due to the shear fracture of the bolts at a deflection of 50 mm, as shown in Figure 28a. Following a practical evaluation of the performance of 1HFRP-G60-4PL-S35, 2HFRP-G60-4PL-S35, and 4HFRP-G60-4PL-S35, the use of a single HFRP strip in the strengthening process to optimize the ductility and the cost of the system is recommended. Using two HFRP strips is expected to increase the cost without remarkable improvement in the yield load (from 2.6% to 5.3%) and the ultimate load (from 18.7% to 21.5%).

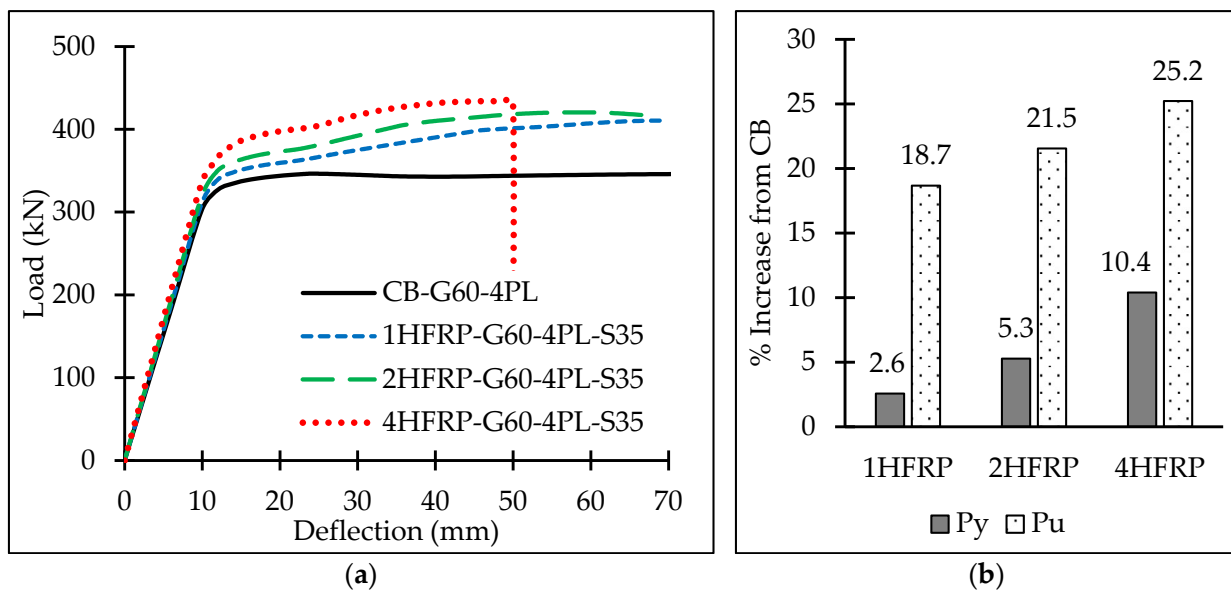


Figure 28. Effect of HFRP thickness with 35 mm spacing in G60 steel beams: (a) load-deflection curves; (b) % increase in yield and ultimate loads from CB.

The effect of the spacing between the bolts was assessed by comparing the plots in Figure 27 to their counterparts in Figure 28. Increasing the connectivity between the bolted HFRP strips and the steel beam by adopting small spacing between the bolts (i.e., 35 mm) enhanced the ductility of the beams, as was made evident by the delayed failure of 2HFRP-G60-4PL-S35 and 4HFRP-G60-4PL-S35 compared to 2HFRP-G60-4PL-S100 and 4HFRP-G60-4PL-S100. It is worth noting that reducing the spacing between the bolts while utilizing a single HFRP strip had an insignificant effect on the ductility and a minor impact on the yield and ultimate load capacities of the strengthened beam, as observed by comparing the behavior of 1HFRP-G60-4PL-S100 and 1HFRP-G60-4PL-S35 models. Therefore, following an economical assessment, the adoption of a spacing of 100 mm between the bolts while using a single HFRP strip is suggested.

4.3.2. Steel Grade

The application of the strengthening technique on steel beams made of A36 steel with the same geometrical and fastening configuration was studied numerically. The mechanical properties of A36 steel reported in the “Standard Specification for Carbon Structural Steel” [47] were incorporated into the model with a yield strength of 250 MPa and an ultimate strength of 400 MPa while maintaining an elastic modulus of 180 GPa. The steel tangential modulus E_t was set to a value of 3.1% E (5580 MPa), as recommended by Salmon et al. [43]. The multi-linear stress-strain curve displayed in Figure 22 was adjusted to reflect the behavior of the A36 steel by using the ϵ_2 of 0.01361, according to [43]. Seven FE models were developed utilizing the A36 steel beams: one un-strengthened control beam (CB); three models with one, two, and four HFRP strips fastened by 100 mm spaced bolts; and three additional models with one, two, and four HFRP strips fastened by 35 mm spaced bolts. The modeled beams were subjected to 4PL while maintaining the original length of the experimental beam with a clear span of 1800 mm. The effects of the HFRP thickness and the spacing between the bolts while strengthening beams made of A36 steel were evaluated. Comparing the ultimate loads of the models to their counterparts in the reference set reflected the effectiveness of the adopted strengthening technique on both steel grades.

Fastening a single HFRP strip to the A36 steel beam while using 100 mm spacing showed 2.2% and 11.6% improvements in the yield and ultimate loads from the CB, respectively, as shown in Figure 29. Although increasing the thickness of the bolted HFRP

to two and four layers slightly improved the yield strength of the system, it adversely affected its ultimate load-carrying capacity due to the BSF reflected in the load-deflection curves in Figure 29a. Typically, increasing the HFRP thickness enhanced the contribution of the HFRP in resisting the applied loads; however, the steel bolts reached their maximum shear capacities due to the insufficient number of bolts. Therefore, increasing the HFRP thickness without maintaining a proper number of bolts reduced the ductility of the system. It is noteworthy that the FE model predicted web local buckling (WLB) at the edge-segment where the shear stresses were generated along with LTB in 4HFRP-A36-S100, as shown in Figure 30b, causing early system failure, while only LTB was predicted in the 2HFRP-A36-S100 model (see Figure 30a).

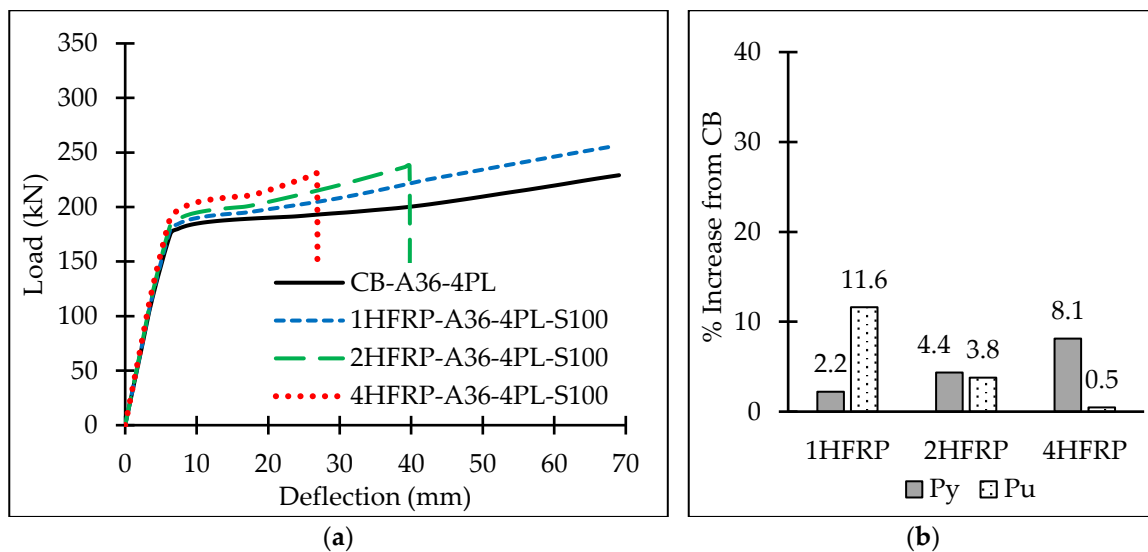


Figure 29. Effect of HFRP thickness with 100 mm spacing in A36 steel beams: (a) load-deflection curves; (b) % increase in yield and ultimate loads from CB.

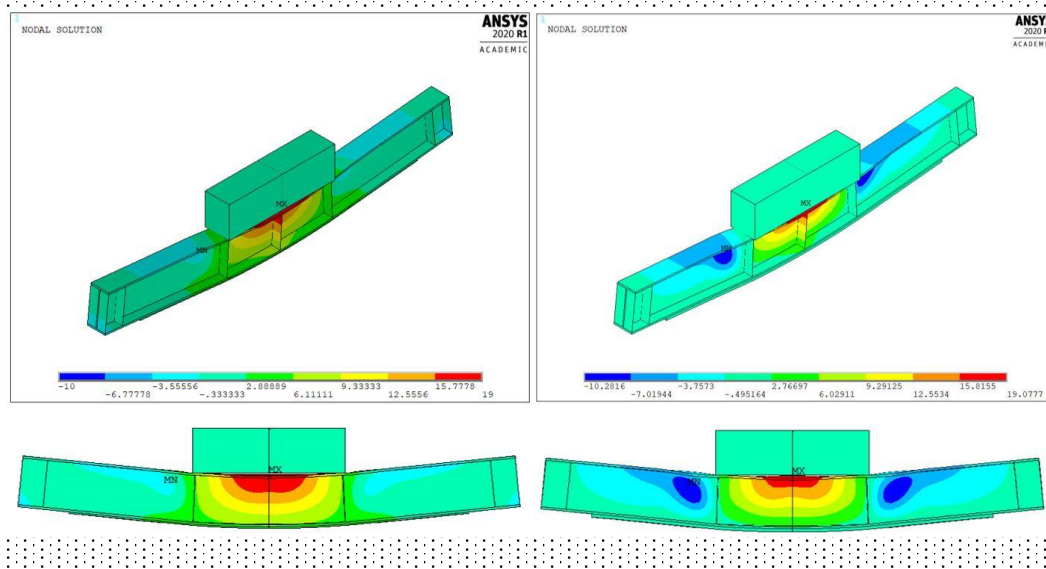


Figure 30. Numerical lateral deflections of: (a) 2HFRP-A36-4PL-S100; (b) 4HFRP-A36-4PL-S100.

Reducing the spacing between the bolts to 35 mm improved the yield and ultimate load capacities of the beams and enhanced the system ductility, as is made evident by comparing the plots in Figures 29 and 31. Fastening one, two, and four strips of the HFRP to a steel beam made of A36 steel using 35 mm spaced bolts enhanced the yield strength of the system by 3.8%, 7.0%, and 11.4%, respectively. Moreover, remarkable improvements of

21.6%, 29.8%, and 34.5% were calculated in the ultimate strength of the beams strengthened by one, two, and four HFRP strips, respectively (see Figure 31b). Although model 4HFRP-A36-4PL-S35 showed significant improvements in the yield and ultimate load capacities, the system failed due to BSF within the plastic zone. Therefore, the optimum ductile performance for similar strengthening conditions with A36 steel can be achieved by using two HFRP strips fastened to the bottom flange of the steel beam using 35 mm spacing between the steel bolts.

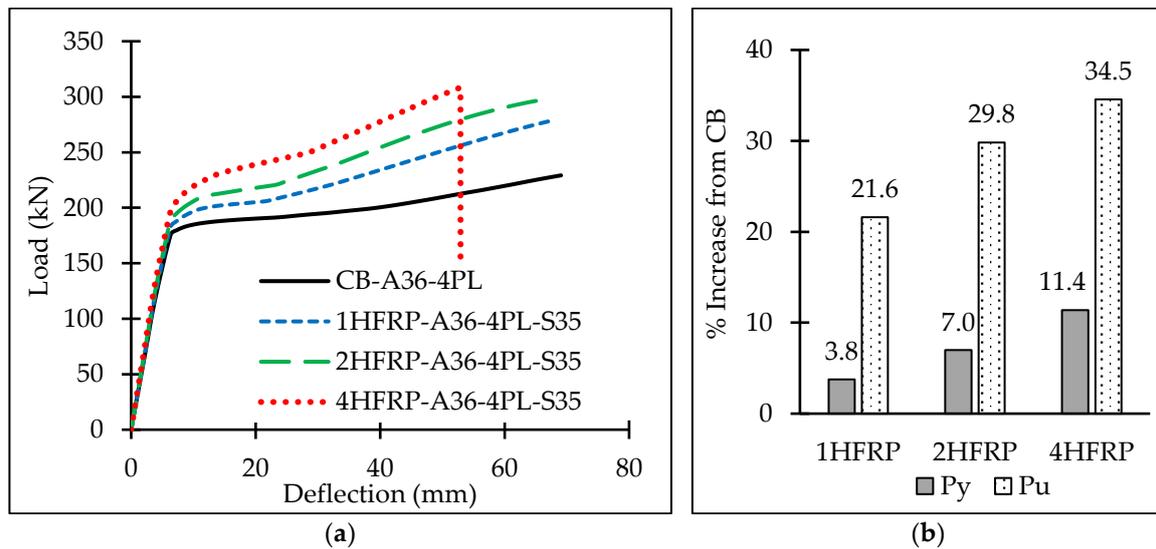


Figure 31. Effect of HFRP thickness with 35 mm spacing in A36 steel beams: (a) load-deflection curves; (b) % increase in yield and ultimate loads from CB.

The ultimate loads of the FE models made of A36 steel and those made of G60 steel in the reference set are displayed in Figure 32. The reported enhancements in the ultimate loads of the G60 steel were higher than those of the A36 steel while maintaining a 100 mm spacing between the bolts (see Figure 32a) due to the flexural failure of the steel beams made of A36 steel. Meanwhile, the effectiveness of the fastening technique became more pronounced in the A36 steel than the G60 steel regardless of the HFRP thickness when a proper bearing was maintained (i.e., by using 35 mm spacing between the bolts), as made evident by the calculated percentage enhancements in the ultimate loads shown in Figure 32b.

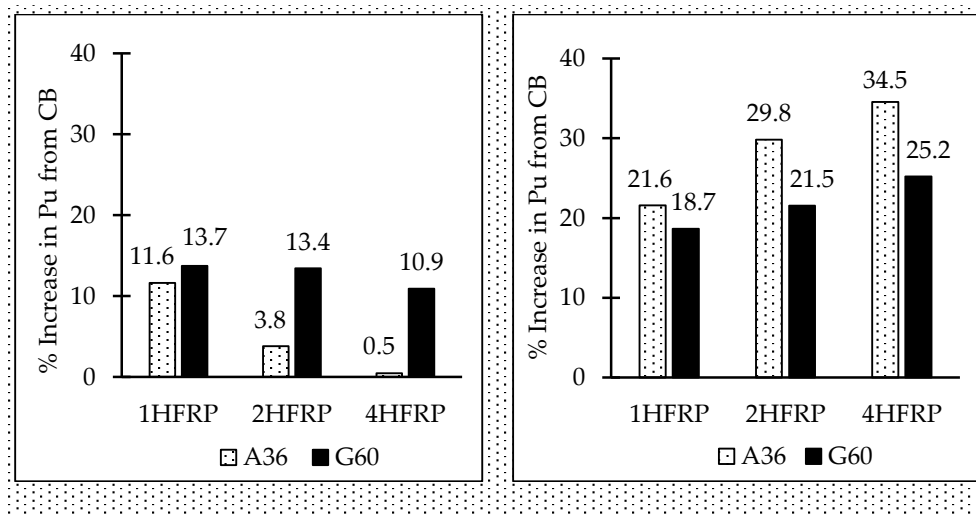


Figure 32. Effect of the steel grade on the ultimate load-carrying capacity with different HFRP thicknesses at: (a) 100 mm and (b) 35 mm spacing between bolts.

4.3.3. Loading Scheme

The experimental findings in Section 3 and the verified FE models in Section 4.2 proved the efficiency of the fastening technique in strengthening steel beams subjected to four-point loading (4PL). This subsection investigates the effectiveness of the adopted fastening technique in enhancing the performance of steel beams subjected to a three-point loading scheme (3PL). The location of the loading nodes was re-defined to model the application of a single-point load at the mid-span of the top steel flange, as shown in Figure 33. Apart from the location of the loading nodes, the geometrical parameters, material modeling, and boundary conditions described in Section 4.1 for the verified FE model were kept unchanged. The effects of the HFRP thickness and the spacing between the bolts under the 3PL scheme were examined.

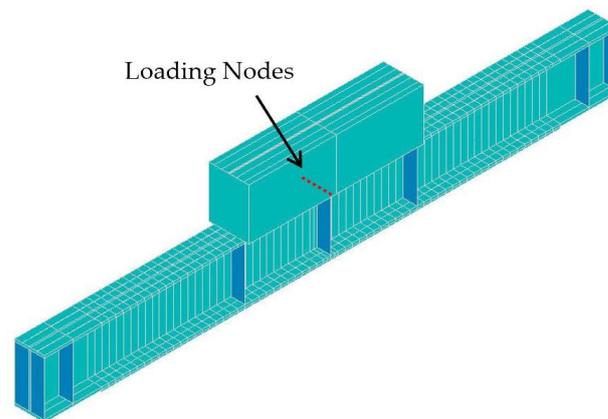


Figure 33. Location of the loading nodes in FE models subjected to 3PL.

The effect of implementing the strengthening technique on steel beams subjected to a 3PL and fastened using 100 mm spaced bolts is shown in Figure 34. A negligible increase in the yield load of the strengthened beams was calculated regardless of the HFRP thickness. Although increasing the HFRP thickness from one strip to two strips slightly improved the ultimate load of the beam (%increase from 5.8 to 8.3%), an additional increase in the HFRP thickness adversely affected the ultimate load due to the early failure of the bolts. It is noteworthy that the configurations subjected to 3PL showed WLB at the mid-segment due to the high shear stresses below the applied load, as shown in Figure 35 for 2HFRP-G60-3PL-S100.

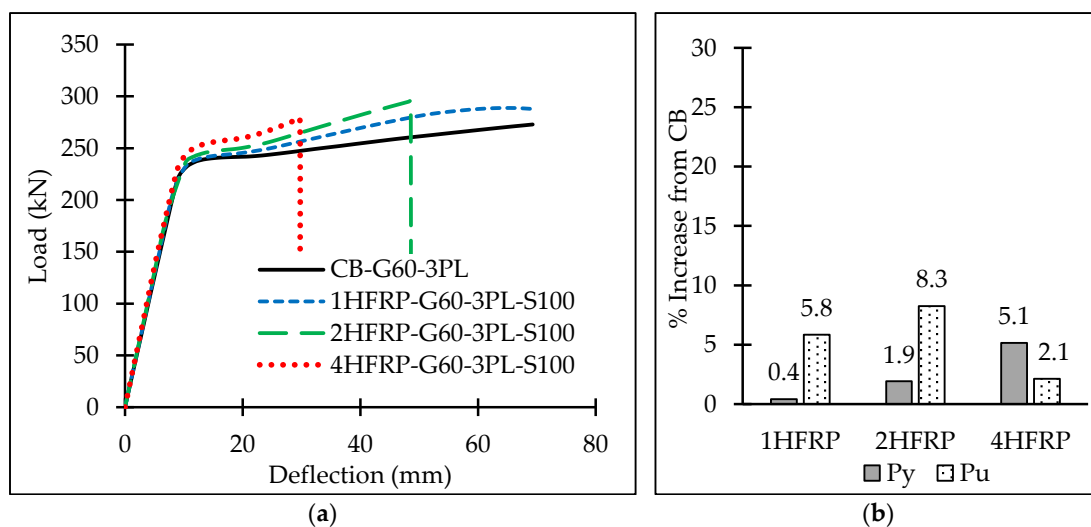


Figure 34. Performance of beams in 3PL with 100 mm spacing: (a) load-deflection curves; (b) % increase in yield and ultimate loads from CB.

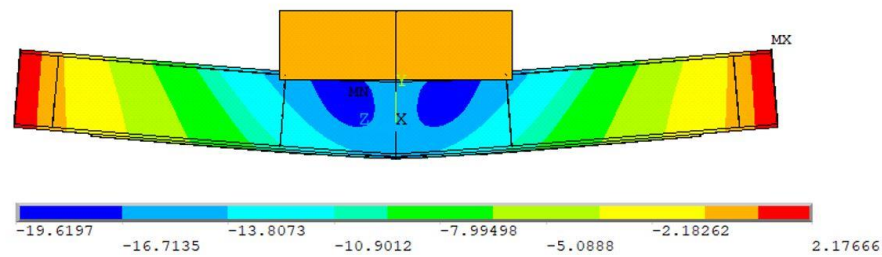


Figure 35. Numerical lateral deformations of 2HFRP-G60-3PL-S100 with WLB at the mid-segment.

Reducing the spacing between the bolts from 100 mm to 35 mm improved the ductility of the system, as made evident by the delayed failure of the bolts in 2HFRP-G60-3PL-S35 and 4HFRP-G60-3PL-S35 shown in Figure 36a compared to those in Figure 34a. The delayed bolt fracture and the improved bearing in the beams fastened by 35 mm spaced bolts resulted in higher enhancements in the yield and ultimate load capacities of the system, as made evident by the calculated percentages in Figure 36b. Model 2HFRP-G60-3PL-S35 offered the optimum performance for the beams subjected to 3PL in terms of ultimate load-carrying capacity and ductility.

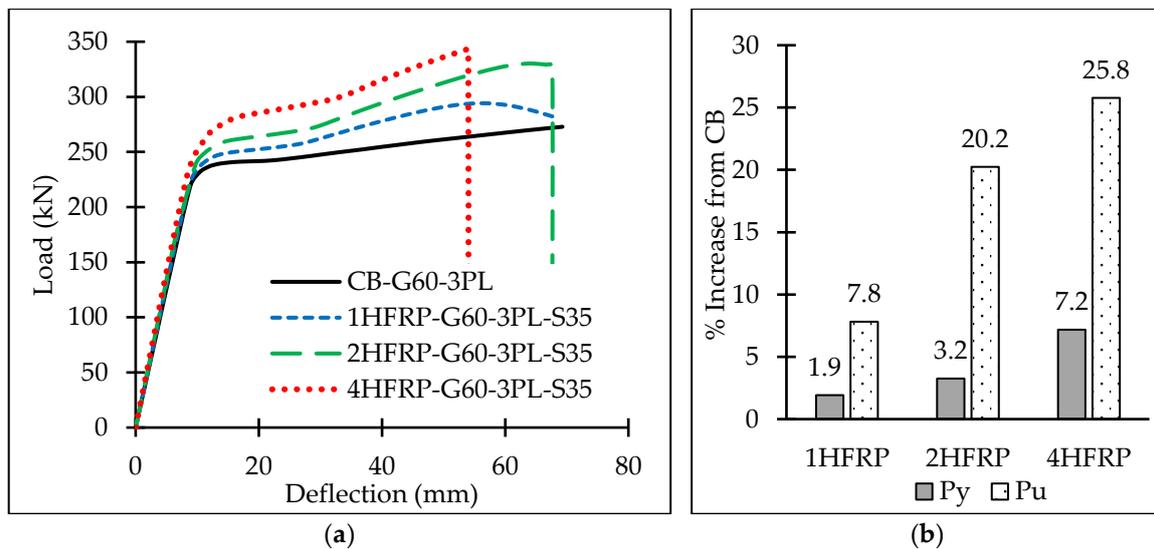


Figure 36. Performance of beams in 3PL with 35 mm spacing: (a) load-deflection curves; (b) % increase in yield and ultimate loads from CB.

The beams subjected to 3PL showed lower ultimate load-carrying capacities than those in 4PL, as shown in Figure 37, at both spacing values. This observation agrees with the findings in [48–50] for different materials tested in 3PL and 4PL schemes. The combined effects of the flexure and shear stresses in the vicinity of the loading point in the 3PL scheme resulted in higher stresses in the beam compared to the 4PL scheme. A proper clarification of the differences between the two loading schemes (i.e., 3PL and 4PL) is provided in view of the generated stresses and their distribution along the beam. Figure 38 shows the shear stresses in the ZY-plane and the flexure stresses in the Z-direction of the CB under 3PL at 240 kN. Consider two elements from the web at the mid-segment of the beam where points “A” and “B” are located above and below the neutral axis, respectively. The stresses in element “A” involve both shear and compressive flexural stresses, whereas the stresses in element “B” display shear and tensile flexural stresses. Meanwhile, in the 4PL scheme, the stresses at the same locations are flexural stresses only, as shown in Figure 39 for the CB in 4PL at 340 kN. The absence of the shear stresses in the mid-segment under 4PL preserved the nominal capacity of the beam and enabled the carrying of higher loads. In other words, the high flexure stresses generated in the 3PL ($M_{3PL} = \frac{PL}{4}$) reduce the effective

area of the web that resists the shear stresses as the flexure stresses penetrate gradually from the flanges into the web [51]. Meanwhile, the application of 4PL generates lower flexure stresses at the same load ($M_{4PL} = \frac{PL}{6}$), enabling the web to preserve its shear capacity to support the structural element at higher loads.

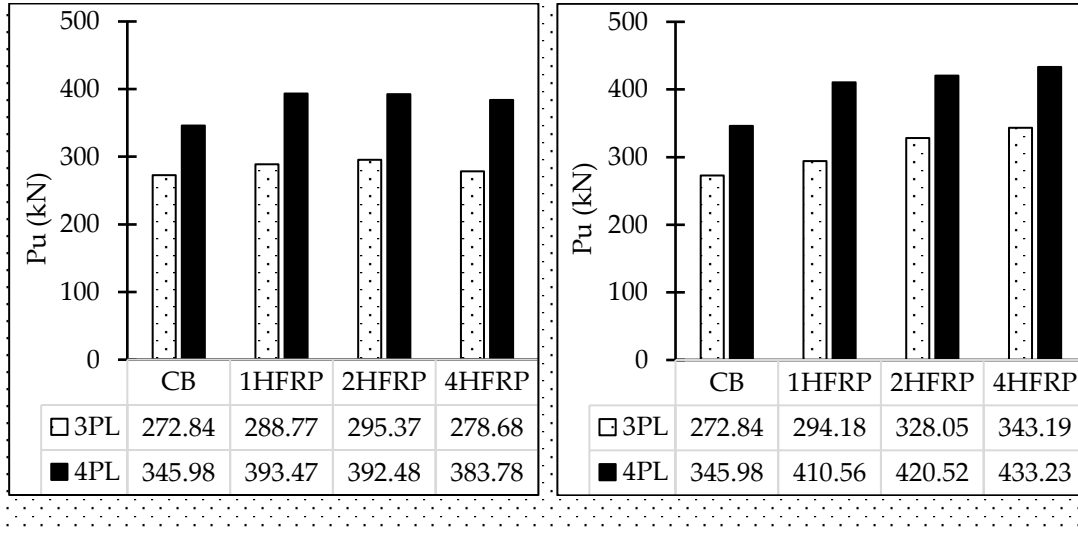


Figure 37. Ultimate loads of beams subjected to 3PL and 4PL at: (a) 100 mm and (b) 35 mm spacing between bolts.

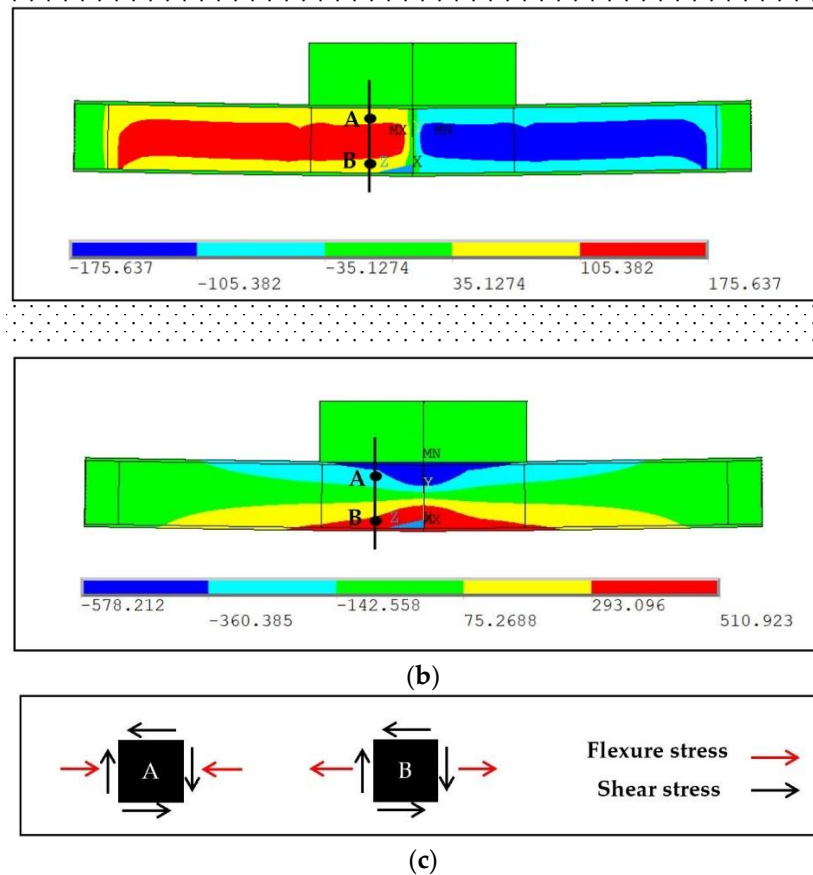


Figure 38. FE stresses in CB in 3PL at 240 kN: (a) shear stresses in YZ-plane; (b) flexure stresses in Z-direction; (c) stress elements at points A and B.

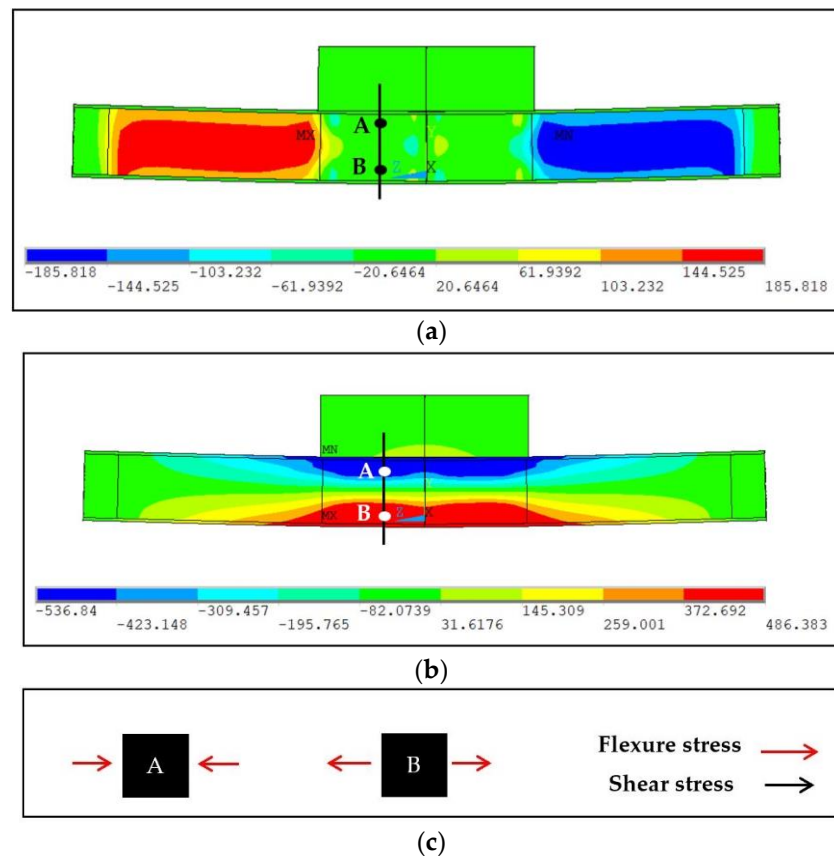


Figure 39. FE stresses in CB in 4PL at 340 kN: (a) shear stresses in YZ-plane; (b) flexure stresses in Z-direction; (c) stress elements at points A and B.

4.3.4. Beam Length

The effectiveness of applying the fastening technique for steel beams with double the clear span tested experimentally in Section 3 was also investigated. The geometrical parameters of the verified FE model were adjusted to model a steel beam with a clear span of 3600 mm while maintaining similar material modeling and boundary conditions. The modeled beams were subjected to 4PL, where the loading nodes were located at 600 mm to the left and the right of the mid-span, as shown in Figure 40. The stiffeners were modeled at the supports, at the mid-span, below the loading points, and at the beam ends in a similar layout to the verified model. It should be noted that the HFRP length in the strengthened beams was increased to maintain a length that was 90% of the clear span. Accordingly, the number of steel bolts was increased to properly fasten the entire length of the HFRP strip to the bottom flange while maintaining a constant spacing between the bolts and a constant shear-edge distance of 50 mm. The effects of the HFRP thickness and the spacing between the bolts were also investigated for the long beams. The designation of this set of beams ends with “2L” to reflect the doubled clear span of the beam relative to the tested specimens.

The load-deflection curves for the beams with double clear span that were strengthened by fastening HFRP strips of various thicknesses using 100 mm spaced steel bolts are displayed in Figure 41. Increasing the HFRP thickness from 1HFRP to 2HFRP increased the yield and ultimate capacities of the system from 2.8% to 5.7% and from 11.2% to 18.4%, respectively. Despite the shear fracture in the bolts of 4HFRP-G60-4PL-S100-2L, a considerable improvement of 11.4% in the yield strength of the system occurred.

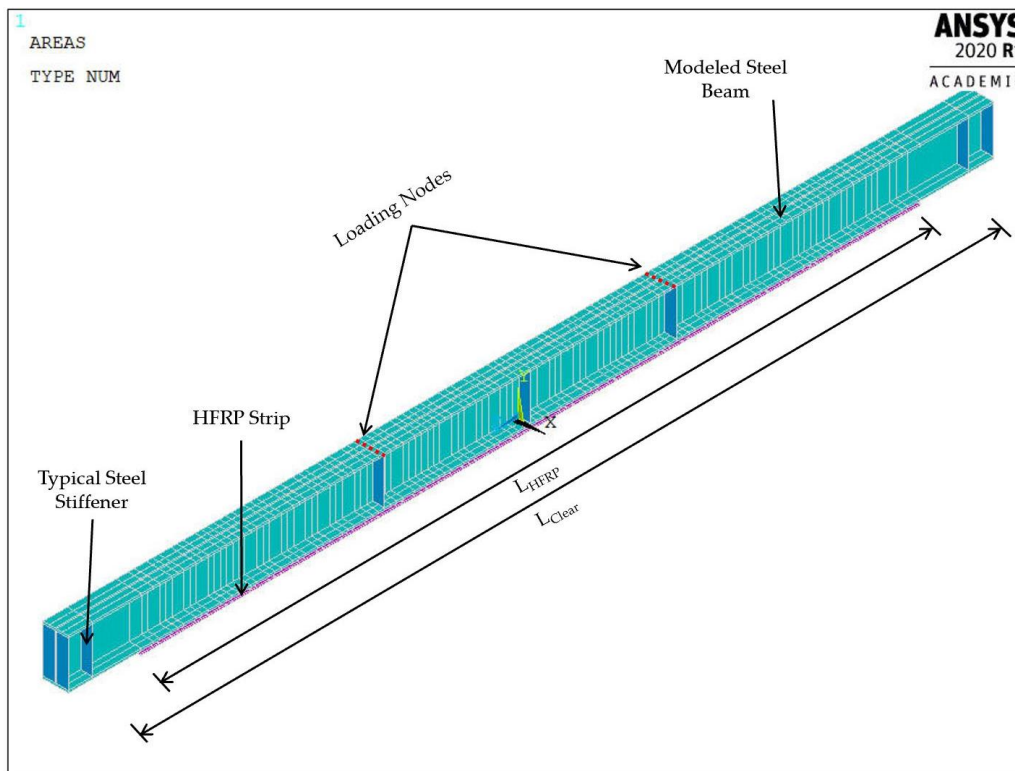


Figure 40. General geometry of the modeled HFRP–steel beam with a double clear span.

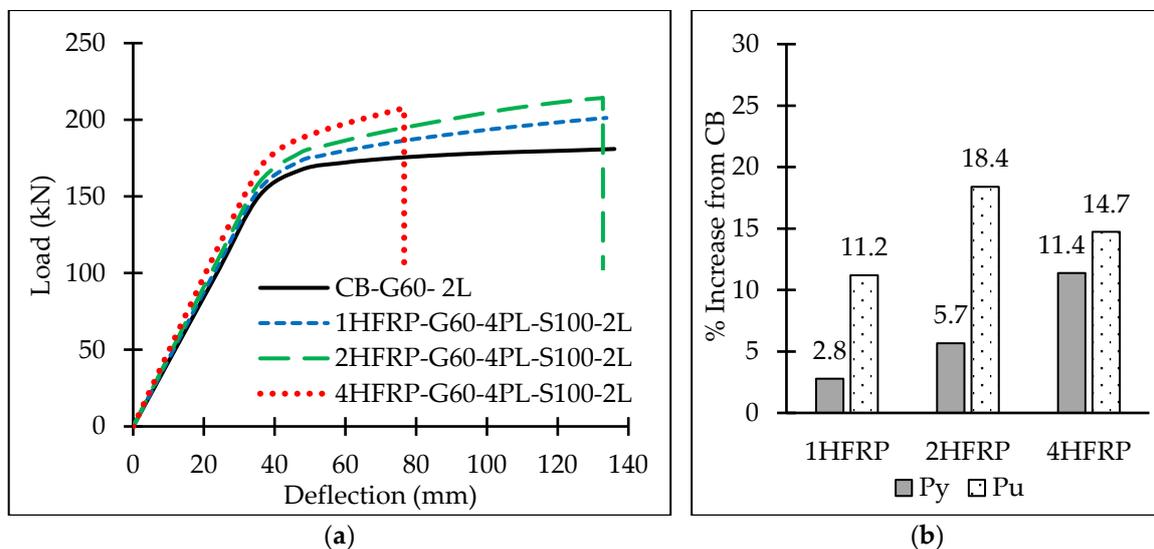


Figure 41. Performance of beams with double clear span with 100 mm spacing: (a) load-deflection curves; (b) % increase in yield and ultimate loads from CB.

Reducing the spacing between the bolts in the long beams enhanced the ductility of the system, as observed by comparing the load-deflection curves in Figure 42a to those in Figure 41a. The improved ductility is also associated with enhancement in the ultimate load-carrying capacity of the beams, as implied by the 27.5% improvement in the ultimate strength of the beam (see Figure 42). The fastening conditions of 4HFRP-G60-4PL-S35-2L promote the optimum performance of the long strengthened beams in terms of ductility, yield load-carrying capacity and ultimate load-carrying capacity.

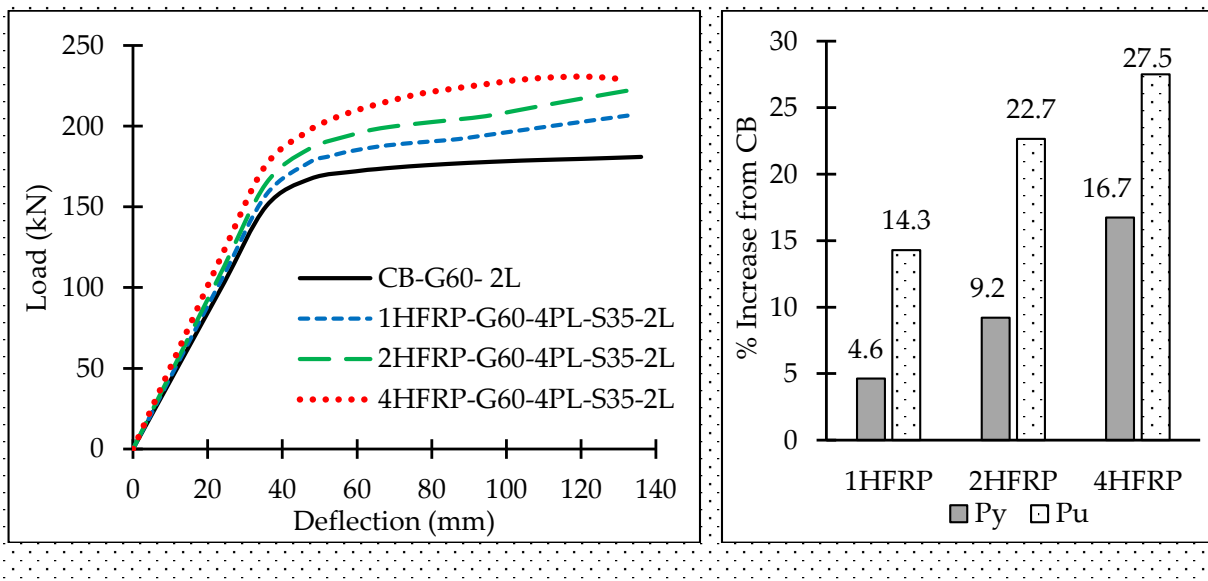


Figure 42. Performance of beams with double clear span with 35 mm spacing: (a) load-deflection curves; (b) % increase in yield and ultimate loads from CB.

Figure 43 compares the percentage increase in the ultimate load of the CB calculated for the long beams with double the clear span to those of the reference set. The ultimate load enhancement for the long beams utilizing a single HFRP strip was slightly lower than that calculated for the short beam at both spacing values as the system's failure in the long beam was governed by the steel material. Meanwhile, increasing the thickness of the HFRP strips in the long beam showed a slight improvement in the ultimate load compared to the short beam at both bolt spacing values. It is worth noting that the increased number of bolts in the long beams enhanced the bearing between the fastened components and the ductility of the system. The effect of the improved ductility was more apparent in the thick HFRP strips (2HFRP and 4HFRP), causing higher improvements in the ultimate load of the long beams than the short beams. In general, the differences in the enhancements of the ultimate loads when considering the long and short beams are insignificant.

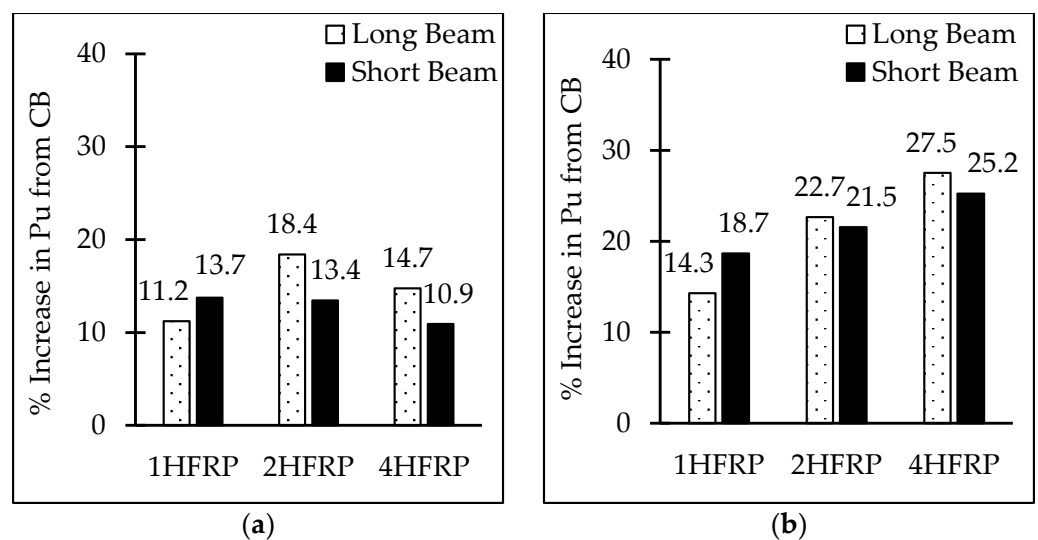


Figure 43. Effect of the beam length on ultimate load-carrying capacity with different HFRP thicknesses at: (a) 100 mm and (b) 35 mm spacing between bolts.

5. Conclusions

The flexural performance of the steel beams strengthened by purely bolted HFRP strips was experimentally and numerically investigated. Twenty-two full-scale beams were tested in a four-point loading setup to assess the effect of the HFRP length and bolt arrangements on the behavior of the strengthened beams. The observed failure modes and the obtained load-deflection curves, deflection profiles, and strain measurements were used to evaluate the effect of the tested parameters. Empirical equations were developed to facilitate the prediction of the ultimate load of the bolted HFRP–steel beams and to anticipate the load-deflection behavior of similar strengthened beams. All the tested configurations were modeled numerically using ANSYS. The developed models showed good agreement with the experimental data, with a yield load error ranging from 0.05% to 2.95% and an ultimate load error ranging from 0.07% to 10.22%. The verified finite element model was used to extend the spectrum of study parameters through an extensive parametric analysis. Such parameters included HFRP thickness, bolt spacing, steel grade, loading scheme, and beam length. The main findings of the conducted experimental and numerical investigations are outlined in the following:

1. Steel beams strengthened by bolted HFRP strips showed ductile behavior while experiencing steel yielding, bearing between the bolts and the HFRP, lateral torsional buckling, and flange local buckling. However, a sufficient number of bolts should be provided to avoid the possibility of shear fracture in the bolts.
2. The proposed fastening technique resulted in significant enhancements in the flexural performance of the strengthened beams, with 15.1% and 22.2% increases in the yield and ultimate flexural capacities compared to the control beam.
3. Better utilization of the HFRP strength was achieved by utilizing long HFRP strips.
4. Increasing the length of the HFRP strip from 45% to 90% of the beam span slightly improved the yield and ultimate flexural capacities of the system. However, it significantly enhanced the ductility of the system and provided better utilization of the bolted HFRP. A 51.2% reduction in the mid-span deflection was attained by increasing the length of the double HFRP strips from 45% to 90% of the beam span.
5. The arrangement of the steel bolts did not show a considerable effect on the yield load, ultimate load, ductility, HFRP utilization, and strain compatibility of the bolted components.
6. The plotted strain profiles proved the effectiveness of the fastening technique in reducing the strains at the bottom steel flange of the strengthened beams. Better strain compatibility and lower slippage were attained by increasing the length of the bolted HFRP strip. Meanwhile, the flexural strains along the bolted HFRP strips followed the distribution of the bending moment along the strengthened beams.
7. Increasing the HFRP thickness without maintaining a proper number of bolts risked the ductility of the system and reduced its ultimate capacities due to the shear fracture of the bolts. Meanwhile, providing a sufficient number of bolts by reducing the bolt spacing enhanced the performance of the strengthened beams.
8. Applying the fastening technique to beams made of A36 steel showed 11.4% and 34.5% improvement in the yield and ultimate loads compared to the control beam, respectively. The study recommends reducing the spacing between the bolts while strengthening the A36 steel beams to avoid shear fracture of the bolts.
9. The beams subjected to three-point loading showed lower yield and ultimate load-carrying capacity than those subjected to four-point loading. This is attributed to the high shear stresses induced in the three-point loading conditions and, consequently, the high combined stresses induced in the beam's section.
10. The numerical study proved the effectiveness of the fastening technique in enhancing the performance of the strengthened beams regardless of the beam length. Strengthening a steel beam with a span of 3600 mm using four HFRP strips with 35 mm spaced steel bolts showed a 27.5% improvement in the ultimate load compared to the control beam.

Author Contributions: Conceptualization, A.M.I.S. and O.R.A.-H.; methodology, A.M.I.S. and O.R.A.-H.; investigation, O.R.A.-H. and A.M.I.S.; validation, O.R.A.-H., A.M.I.S. and K.M.E.-S.; formal analysis, O.R.A.-H. and A.M.I.S.; resources, A.M.I.S.; software, O.R.A.-H., A.M.I.S. and K.M.E.-S.; data curation, O.R.A.-H.; writing—original draft preparation, O.R.A.-H.; writing—review and editing, A.M.I.S. and B.E.-A.; visualization, O.R.A.-H. and A.M.I.S.; supervision, A.M.I.S., B.E.-A. and K.M.E.-S.; project administration, A.M.I.S.; funding acquisition, A.M.I.S. All authors have read and agreed to the published version of the manuscript.

Funding: This research is funded by the Emirates Center for Mobility Research (ECMR) at UAE University, grant number 31R083.

Data Availability Statement: The data presented in this study are available on request from the corresponding author.

Acknowledgments: The authors would like to acknowledge the technical support provided by Engineer Tarek Salah, the senior laboratory specialist in the Structures Laboratory at UAE University.

Conflicts of Interest: The authors declare no conflict of interest.

References

1. Zeng, J.-J.; Gao, W.-Y.; Liu, F. Interfacial behavior and debonding failures of full-scale CFRP-strengthened H-section steel beams. *Compos. Struct.* **2018**, *201*, 540–552. [\[CrossRef\]](#)
2. Teng, J.G.; Yu, T.; Fernando, D. Strengthening of steel structures with fiber-reinforced polymer composites. *J. Constr. Steel Res.* **2012**, *78*, 131–143. [\[CrossRef\]](#)
3. Tafsirojjaman, T.; Ur Rahman Dogar, A.; Liu, Y.; Manalo, A.; Thambiratnam, D.P. Performance and design of steel structures reinforced with FRP composites: A state-of-the-art review. *Eng. Fail. Anal.* **2022**, *138*, 106371. [\[CrossRef\]](#)
4. Bastani, A.; Das, S.; Kenno, S. Rehabilitation of thin walled steel beams using CFRP fabric. *Thin-Walled Struct.* **2019**, *143*, 106215. [\[CrossRef\]](#)
5. Hussein, L.F.; Abbas, F.S.; Al-Balhawi, A.; AL-Ridha, A.S.D.; Hussein, H.H. Investigating the elastic and plastic behavior of I-steel beams by using carbon fiber laminates. *Mater. Today Proc.* **2021**, *56*, 2714–2720. [\[CrossRef\]](#)
6. Borrie, D.; Al-Saadi, S.; Zhao, X.-L.; Raman, R.K.S.; Bai, Y. Bonded CFRP/Steel Systems, Remedies of Bond Degradation and Behaviour of CFRP Repaired Steel: An Overview. *Polymers* **2021**, *13*, 1533. [\[CrossRef\]](#) [\[PubMed\]](#)
7. Pang, Y.; Wu, G.; Wang, H.; Su, Z.; He, X. Experimental study on the bond behavior of CFRP-steel interfaces under quasi-static cyclic loading. *Thin-Walled Struct.* **2019**, *140*, 426–437. [\[CrossRef\]](#)
8. Hu, B.; Li, Y.; Jiang, Y.-T.; Tang, H.-Z. Bond behavior of hybrid FRP-to-steel joints. *Compos. Struct.* **2020**, *237*, 111936. [\[CrossRef\]](#)
9. Wang, Z.; Li, C.; Sui, L.; Xian, G. Effects of adhesive property and thickness on the bond performance between carbon fiber reinforced polymer laminate and steel. *Thin-Walled Struct.* **2021**, *158*, 107176. [\[CrossRef\]](#)
10. Katrizadeh, E.; Narmashiri, K. Experimental study on failure modes of MF-CFRP strengthened steel beams. *J. Constr. Steel Res.* **2019**, *158*, 120–129. [\[CrossRef\]](#)
11. Kumaraguru, S.; Alagusundaramoorthy, P. Flexural strengthening of steel beams using pultruded CFRP composite sheets with anchorage mechanisms. *Structures* **2021**, *33*, 1414–1427. [\[CrossRef\]](#)
12. Al-Ridha, A.S.D.; Hameed, Q.K.; Atshan, A.F.; Abbood, A.A.; Dheyab, L.S. Evaluation of Strengthening Steel Beams Using the Technique of Carbon Fiber Confinement by a Steel Plate (CFCSP). *Adv. Civ. Eng. Mater.* **2020**, *9*, 53–66. [\[CrossRef\]](#)
13. Esmaeeli, E.; Shadan, P. Effectiveness of Fan Anchors in Preventing Debonding in FRP-Strengthened Steel Members. *Int. J. Steel Struct.* **2022**, *23*, 96–119. [\[CrossRef\]](#)
14. Siwowski, T.W.; Siwowska, P. Experimental study on CFRP-strengthened steel beams. *Compos. Part B Eng.* **2018**, *149*, 12–21. [\[CrossRef\]](#)
15. Siwowski, T.; Piątek, B.; Siwowska, P.; Wiater, A. Development and implementation of CFRP post-tensioning system for bridge strengthening. *Eng. Struct.* **2020**, *207*, 110266. [\[CrossRef\]](#)
16. Yang, Y.; Zhao, J.; Zhang, S.; Chastre, C.; Biscaia, H. Effect of mechanical anchorage on the bond performance of double overlapped CFRP-to-steel joints. *Compos. Struct.* **2021**, *267*, 113902. [\[CrossRef\]](#)
17. Li, J.; Wang, Y.; Deng, J.; Jia, Y. Experimental study on the flexural behaviour of notched steel beams strengthened by prestressed CFRP plate with an end plate anchorage system. *Eng. Struct.* **2018**, *171*, 29–39. [\[CrossRef\]](#)
18. Deng, J.; Fei, Z.; Li, J.; Li, H. Fatigue behaviour of notched steel beams strengthened by a self-prestressing SMA/CFRP composite. *Eng. Struct.* **2023**, *274*, 115077. [\[CrossRef\]](#)
19. Li, Z.; Zhao, Q.; Wu, Y.; Zhu, Y.; Wang, H. A theoretical and experimental study on the pre-tensioning and anchorage of composite materials based on shape memory alloys. *Case Stud. Constr. Mater.* **2023**, *18*, e01599. [\[CrossRef\]](#)
20. Ghafoori, E.; Motavalli, M. Innovative CFRP-Prestressing System for Strengthening Metallic Structures. *J. Compos. Constr.* **2015**, *19*, 04015006. [\[CrossRef\]](#)

21. Kianmofrad, F.; Ghafoori, E.; Elyasi, M.; Motavalli, M.; Rahimian, M. Strengthening of metallic beams with different types of pre-stressed unbonded retrofit systems. *Compos. Struct.* **2017**, *159*, 81–95. [[CrossRef](#)]
22. Hosseini, A.; Ghafoori, E.; Motavalli, M.; Nussbaumer, A.; Zhao, X.L.; Al-Mahaidi, R. Flat pre-stressed unbonded retrofit system for strengthening of existing metallic I-Girders. *Compos. Part B Eng.* **2018**, *155*, 156–172. [[CrossRef](#)]
23. Hai, N.D.; Mutsuyoshi, H. Structural behavior of double-lap joints of steel splice plates bolted/bonded to pultruded hybrid CFRP/GFRP laminates. *Constr. Build. Mater.* **2012**, *30*, 347–359. [[CrossRef](#)]
24. Sweedan, A.M.I.; El-Sawy, K.M.; Alhadid, M.M.A. Interfacial behavior of mechanically anchored FRP laminates for strengthening steel beams. *J. Constr. Steel Res.* **2013**, *80*, 332–345. [[CrossRef](#)]
25. Yun, J.-H.; Choi, J.-H.; Kweon, J.-H. A study on the strength improvement of the multi-bolted joint. *Compos. Struct.* **2014**, *108*, 409–416. [[CrossRef](#)]
26. El-Sisi, A.E.-D.; Sallam, H.E.-D.; Salim, H.A.; El-Husseiny, O.M. Structural behavior of hybrid CFRP/steel bolted staggered joints. *Constr. Build. Mater.* **2018**, *190*, 1192–1207. [[CrossRef](#)]
27. Abou El-Hamd, O.R.; Sweedan, A.M.I.; El-Sawy, K.M. Experimental and numerical study of the parameters controlling the behavior of double-lap connections of steel plates bolted to hybrid FRP strips. *Thin-Walled Struct.* **2018**, *125*, 140–151. [[CrossRef](#)]
28. Liu, K.; Liu, Y.; Sabbrojjaman, M.; Tafsirojjan, T. Effect of bolt size on the bearing strength of bolt-connected orthotropic CFRP laminate. *Polymer Test.* **2023**, *118*, 107894. [[CrossRef](#)]
29. El-Sisi, A.E.-D.A.; El-Emam, H.M.; Salim, H.A.; Sallam, H.E.-D.M. Deformation and load transfer analysis of staggered composite-steel lap joints subjected to progressive damage. *Eng. Struct.* **2020**, *215*, 110690. [[CrossRef](#)]
30. Jiang, Z.; Wan, S.; Fang, Z.; Song, A. Static and fatigue behaviours of a bolted GFRP/steel double lap joint. *Thin-Walled Struct.* **2020**, *158*, 107170. [[CrossRef](#)]
31. Sweedan, A.M.I.; Alhadid, M.M.A.; El-Sawy, K.M. Experimental study of the flexural response of steel beams strengthened with anchored hybrid composites. *Thin-Walled Struct.* **2016**, *99*, 1–11. [[CrossRef](#)]
32. Sweedan, A.M.I.; Rojob, H.N.; El-Sawy, K.M. Mechanically-fastened hybrid composites for flexural strengthening of steel beams. *Thin-Walled Struct.* **2014**, *85*, 250–261. [[CrossRef](#)]
33. Sweedan, A.M.I.; Rojob, H.N.; El-Sawy, K.M. Analytical and numerical study of the serviceability performance of partial composite steel-FRP beams. *Int. J. Struct. Integr.* **2018**, *9*, 625–645. [[CrossRef](#)]
34. About El-Hamd, O.R.; Sweedan, A.M.I.; El-Ariss, B. Flexural Performance of Steel Beams Strengthened by Fastened Hybrid FRP Strips Utilizing Staggered Steel Bolts. *Buildings* **2022**, *12*, 2150. [[CrossRef](#)]
35. *ASTM Standard A370-21*; Standard Test Methods and Definitions for Mechanical Testing of Steel Products. American Society of Testing Materials (ASTM) Standards: West Conshohocken, PA, USA, 2021.
36. Strongwell Manufacturing Plants. *SAFSTRIP: Fiber Reinforced Strengthening Strip*; Strongwell: Chatfield, MN, USA, 2020.
37. *DIN EN ISO 4017*; Fasteners—Hexagon Head Screws—Product Grades A and B. DIN-Adopted European-Adopted ISO Standards. Deutsches Institut für Normung (DIN) Standards: Berlin, Germany, 2014.
38. Youssef, M.A. Analytical prediction of the linear and nonlinear behaviour of steel beams rehabilitated using FRP sheets. *Eng. Struct.* **2006**, *28*, 903–911. [[CrossRef](#)]
39. Kamruzzaman, M.; Jumaat, M.; Sulong, N.H.R.; Qeshta, I.M.I.; Narmashiri, K. Effects of Lateral Bracing and Stiffeners on the CFRP Failure of Strengthened Steel Beams. *IOP Conf. Ser. Mater. Sci. Eng.* **2017**, *210*, 12021. [[CrossRef](#)]
40. Peiris, A.; Harik, I. Steel beam strengthening with UHM CFRP strip panels. *Eng. Struct.* **2021**, *226*, 111395. [[CrossRef](#)]
41. El Damatty, A.A.; Abushagur, M.; Youssef, M.A. Experimental and analytical investigation of steel beams rehabilitated using GFRP sheets. *Steel Compos. Struct.* **2003**, *3*, 421–438. [[CrossRef](#)]
42. Ansys®. *Mechanical APDL*; Help System; ANSYS, Inc.: Canonsburg, PA, USA, 2020.
43. Salmon, C.G.; Johnson, J.E.; Malhas, F.A. *Steel Structures, Design and Behavior, Emphasizing Load and Resistance Factor Design*, 5th ed.; Pearson Prentice Hall Publishers: Hoboken, NJ, USA, 2009.
44. Foster, A.S.J.; Gardner, L.; Wang, Y. Practical strain-hardening material properties for use in deformation-based structural steel design. *Thin-Walled Struct.* **2015**, *92*, 115–129. [[CrossRef](#)]
45. Kachlakev, D. *Strengthening Bridges Using Composite Materials*; Oregon Department of Transportation Research Unit: Salem, OR, USA, 1998. [[CrossRef](#)]
46. Kachlakev, D.I.; McCurry, D., Jr. *Simulated Full Scale Testing of Reinforced Concrete Beams Strengthened with FRP Composites: Experimental Results and Design Model Verification*; Oregon Department of Transportation: Salem, OR, USA, 2000.
47. *ASTM Standard A36/A36M*; Standard Specification for Carbon Structural Steel. American Society of Testing Materials (ASTM) Standards: West Conshohocken, PA, USA, 2019.
48. Daniel, I.M.; Abot, J.L. Fabrication, testing and analysis of composite sandwich beams. *Compos. Sci. Technol.* **2000**, *60*, 2455–2463. [[CrossRef](#)]
49. Bencardino, F. Mechanical Parameters and Post-Cracking Behaviour of HPFRC According to Three-Point and Four-Point Bending Test. *Adv. Civ. Eng.* **2013**, *2013*, 179712. [[CrossRef](#)]

50. Al-Abtah, F.G.; Mahdi, E.; Gowid, S. The use of composite to eliminate the effect of welding on the bending behavior of metallic pipes. *Compos. Struct.* **2020**, *235*, 111793. [[CrossRef](#)]
51. McCormac, J.C. *Structural Steel Design*, 4th ed.; Pearson Prentice Hall: Hoboken, NJ, USA, 2008.

Disclaimer/Publisher's Note: The statements, opinions and data contained in all publications are solely those of the individual author(s) and contributor(s) and not of MDPI and/or the editor(s). MDPI and/or the editor(s) disclaim responsibility for any injury to people or property resulting from any ideas, methods, instructions or products referred to in the content.